NAL PROPOSAL No. 133

Scientific Spokesman:
W. D. Shephard
Physics Department
University of Notre Dame
Notre Dame, Indiana 46556

Telephone: 219 - 283-7311

# STUDY OF MULTIPION PRODUCTION IN HIGH ENERGY $\pi^- p$ INTERACTIONS AT NAL USING THE 30-IN. HYDROGEN BUBBLE CHAMBER AND A WIDE-GAP SPARK CHAMBER SPECTROMETER

N. N. Biswas, N. M. Cason, V. P. Kenney, J. A. Poirier, C. A. Rey, O. R. Sander, W. D. Shephard, D. W. Thomas, plus graduate students

University of Notre Dame

April 28, 1971

# I. COVER PAGE

Title: STUDY OF MULTIPION PRODUCTION IN HIGH ENERGY $\pi^-p$ INTERACTIONS AT NAL USING THE 30-IN. HYDROGEN BUBBLE CHAMBER AND A WIDE-GAP SPARK CHAMBER SPECTROMETER.

Abstract: We propose to study 300 GeV/c $\pi^-p$ interactions at NAL with a hybrid bubble chamber-optical spark chamber spectrometer system. The inclusive reaction $\pi^-p \rightarrow \pi^-$ + anything will be studied in detail. We will measure distributions of the scaling variable x, the transverse momentum Q, and the charge-multiplicity n and their interdependence over a wider range of x than is otherwise obtainable. These and related distributions will be compared with the predictions of current models for high energy interactions. The experiment will extend Notre Dame measurements at conventional accelerator energies (8 and 18.5 GeV/c) to energies where asymptotic approximations may be valid and discrimination among the models should be possible. In addition we will study those "exclusive" reactions such as target and/or beam diffraction dissociation if cross sections remain significant. We believe that significant results can be obtained within 2-3 months of data acquisition.

Names of Experimenters: N. N. Biswas, N. M. Cason, V. P. Kenney, J. A. Poirier, C. A. Rey, O. R. Sander, W. D. Shephard, and D. W. Thomas, plus graduate students.

Affiliation: University of Notre Dame, Notre Dame, Indiana 46556

Date: April 28, 1971

Spokesman: W. D. Shephard, Physics Department, University of Notre Dame, Notre Dame, Indiana 46556. Telephone: 219-283-7311

TABLE OF CONTENTS PAGE

TABLE OF CONTENTS

## II. SUMMARY

We are proposing a study at NAL of $\pi^-$p reactions at 300 GeV/c in a hybrid system composed of the 30-in. hydrogen bubble chamber, a downstream spectrometer composed of wide-gap optical spark chambers, and an upstream beam-tagging system composed of proportional wire chambers and a Cerenkov counter. The same spectrometer system will be used in other experiments to provide studies of high energy interactions with different beam particles and at different incident momenta. If a beam sufficiently enriched in $\pi^+$ mesons at 300 GeV/c exists, we plan to extend this proposal to provide a study of $\pi^+$p interactions at 300 GeV/c. Notre Dame proposes to provide hardware and software for putting information from proportional chambers and Cerenkov counters in the beam line onto magnetic tape.

In Section III we describe the physics which can result from this experiment. The reactions of interest include the "inclusive" process $\pi^- + p \rightarrow \pi^- +$ anything and also any "exclusive" processes, such as diffraction dissociation of beam or target particles, which may prove to have significant cross sections at this energy. From extrapolation of results we have already obtained at lower energies, we believe that in the proposed experiment: (a) scaling and factorization can be tested at high energies ($s = 564$ GeV$^2$) and, especially, at large positive values of the scaling variable $x$; (b) distributions of the rapidity variable $w$ may provide a distinction between multiperipheral and fragmentation

models; (c) tests can be made of the theory that secondary particles are mainly produced in quark-quark interactions; (d) depending on the trigger used for the downstream spectrometer, fragmentation of projectile and/or target particles can be studied; predictions of thermodynamic models for transverse-momentum distributions can be checked over a large range of Q and x; production of fast forward $\pi^o$ mesons can be studied. The proposed spectrometer will provide additional information, which is unobtainable in a "bare" bubble chamber experiment, on tracks with large laboratory momenta.

In Section IV are described the construction and properties of the hybrid spectrometer to be used in the experiment. In Section V we indicate the justification for the size of the proposed exposure. Finally, in Section VI we demonstrate the capability of Notre Dame to obtain rapid results from the experiment and the capacity of the proposed spectrometer to provide the information needed for significant physics results.

## III. PHYSICS JUSTIFICATION

### A. Introduction.

The study of the characteristics of inelastic processes in hadron-hadron collisions is of considerable interest. At high energies the inelastic processes are dominant, the production of resonances in any specific channel becomes relatively small, and many particles are involved. It is of particular interest[1-5] to study processes such as

$$A + B \rightarrow C + \text{anything}$$

which are, in the terminology of Feynman, "inclusive processes" with no constraints on the final-state products other than the presence of C, the particle being studied. The cross sections for such processes are expected to remain significant as the incident momentum is increased.

Investigations have already been carried out at conventional accelerator energies (below 30 GeV) on the reactions:

$$\pi^{\pm} p \rightarrow \pi^{-} + \text{anything}^{6,7}, \quad (1)$$

$$K^{+} p \rightarrow \pi^{-} + \text{anything}^{8}, \quad (2)$$

$$pp \rightarrow \pi^{-} + \text{anything}^{9}. \quad (3)$$

For example, the Notre Dame group[6] has recently studied $\pi^{\pm}p$ interactions at 8 and 18.5 GeV/c. The results we have obtained are typical of the situation at current accelerator energies. It is expected that results from Serpukhov will soon be available at somewhat higher energies (up to 70 GeV). Further progress will require the results of experiments at NAL such as the experiment proposed here.

Various models of high energy hadron-hadron interactions have been proposed including the parton model[1], limiting-fragmentation model[2],

quark models[7], multiperipheral models[4], thermodynamic models[3] and others[5]. Predictions are made about the distributions of the scaling variable x and the transverse momentum Q. The scaling variable x is defined as $x = p_{\parallel} / p_o$ where $p_{\parallel}$ is the longitudinal momentum of a secondary particle in the overall center-of-mass (c.m.) system and $p_o$ is the c.m. momentum of the incident pion[10]. Data obtained at presently available energies[6-9] reveal some general features of multiparticle interactions that are also observed at cosmic-ray energies and which must be explained by any successful model. These include: (a) small transverse momenta ($< Q > \sim .3 - .5$ GeV/c); (b) relatively low multiplicity ($< n > \sim \ln s$ or $s^{1/4}$); (c) longitudinal momenta $< p_{\parallel} >$ much greater than $< Q >$ at high energies. However, data at NAL energies are needed to distinguish clearly among the models and to establish or disprove predictions such as scaling and factorization.

"Exclusive" processes which are expected to have cross sections large enough for study even at NAL energies include "diffraction dissociation"[11,2] of the target or of the projectile. Cross sections for dissociation into all-charged particles are ~ .1 to 1 mb at current accelerator energies and are expected to remain constant or to decrease only slowly with increasing energy. The energy dependence of these cross sections is thus of considerable interest. The appropriate coordinate system in which to study such dissociation processes is the rest system of the dissociating particle. Measurements must be of sufficient accuracy to eliminate most events involving additional neutral particles.

In order to obtain information about "inclusive" and selected "exclusive" processes for varying multiplicities, a detector with the large solid-angle

of acceptance of the bubble chamber is desirable. Much can be done with a "bare" bubble chamber[12]. However, to cover the full range of secondary momenta expected from incident particles in the 100 GeV range it is necessary to supplement the bubble chamber with a downstream spectrometer system which will provide information about high momentum secondaries ($p \gtrsim 20$ GeV/c) which will be kinematically limited to a small range of angles ($\lesssim 3^{o}$) in the forward direction. This proposal is based on a design for such a hybrid system made up of the 30-in. hydrogen bubble chamber and a wide gap optical spark chamber spectrometer which will initially use the field of the bubble chamber magnet to provide momentum dispersion. The same spectrometer described in Section IV will be used in a number of experiments involving $\pi^{\pm}$p and pp interactions at a variety of incident momenta. Thus our proposed experiment will not only provide information on many points of interest at a single energy, but also can provide data which will be compared with data for events at other incident energies with different incident particles. The coordinated efforts of a variety of university groups should thus provide physics results considerably greater than an incoherent sum of the results of individual experiments.

We request a 300,000 picture exposure at 300 GeV/c incident $\pi^{-}$ momentum with an average of 10 incident particles per picture. Based on extrapolations from our current studies of $\pi^{\pm}$p interactions at 8 and 18.5 GeV/c and on our studies of the capabilities of the hybrid system, the proposed exposure is expected to provide sufficient data for detailed studies of the correlations between x, Q, and n over a wide range of these variables.

Information can be obtained at a much greater range of longitudinal momenta than can be studied without the use of the downstream spectrometer. If it proves possible to obtain beams of positive particles consisting primarily of $\pi^+$ mesons at 300 GeV/c we plan to extend this proposal to include a request for a $\pi^+p$ exposure. This would allow a comparison of $\pi^+p$ and $\pi^-p$ interactions at the same energy and allow the study of "leading particle" effects. In the remainder of this section we relate specific features of the data obtainable in this experiment to the predictions of models and show how this experiment will extend the results expected from "bare" bubble-chamber experiments.

B. Scaling and Factorization: Multiperipheral and Fragmentation Models

The scaling property of momentum distributions, first proposed by Feynman[1], has been found to hold for a variety of models[13-15]. The conjecture is that

$$\frac{2E}{\pi\sqrt{s}}\ \frac{d^2\sigma}{dx dQ^2} = f(x, Q, s) \xrightarrow[s \to \infty]{} f(x, Q)$$

Details vary in the different models[13], but the apparently fundamental nature of the scaling hypothesis makes tests of its validity imperative.

A further hypothesis, that of "factorization", suggests that $f(x, Q)$ can be factorized into independent functions of x and Q for large s. Data at present available energies suggest that, while there appears to be evidence for some form of scaling behavior, there is as yet no quantitative support for factorization. The Notre Dame data for $\pi^{\pm}p \to \pi^-$ + anything at 8 and 18.5 GeV/c have been studied to determine the dependence of the cross section on x and Q. Representative x-distributions are shown in Fig. 1 and $Q^2$ distributions are shown in Fig. 2. The x-distributions exhibit dependence

on Q and on the prong number n; the Q-distributions depend on x and n. To illustrate this dependence, the data have been fitted to expressions of the form

$$dN/dQ = CQ^{3/2} \exp\left[-aQ\right]$$

and

$$dN/dx = C \exp\left[-b|x|\right].$$

The coefficient a has been determined as a function of n and x and the coefficient b as a function of n and $Q^2$ as shown in Fig. 3. The dependence of a on x and of b on $Q^2$, shown in Figs. 3b, d, f and h, indicates that $d^2\sigma/dxdQ^2$ cannot be factorized into independent functions of x and $Q^2$. We also find that $(d^2\sigma/dxdQ^2)E$ cannot be factorized into independent functions of x and $Q^2$. Results consistent with ours have been found for $K^+p$ interactions[8] at 11.8 GeV/c. Since factorization is predicted to hold in the asymptotic limit, high-energy experiments are clearly required.

Values of b are found to differ for $x > 0$ and $x < 0$ in both the $\pi^+p$ (no "leading particle" contribution) and $\pi^-p$ cases[6]. The same is true for $K^+p$ data[8]. For $x < 0$, our values of b for $\pi^+p$ and $\pi^-p$ are similar, and are in qualitative agreement with values for $\pi^-p$ data at 8 and 25 GeV/c and with $K^+p$ and pp data[10] as shown in Table I. For $x < 0$, the values of a are also similar for $\pi^\pm p$ and pp interactions as shown in Table II. (We find that da/dn and db/dn, the slopes of the straight lines in Figs. 3a, c, e, and g, are also in agreement with results for pp interactions.) This suggests that fragmentation of the proton is independent of the projectile particle $\pi^\pm$, $K^+$, or p. Details of the target fragmentation at 300 GeV/c can thus be examined in the proposed experiment. In addition it should be possible to study fragmentation of the projectile in its own rest system with precision considerably greater than

Table I

Values of b Found in

Fits to $dN/dx = C \exp\left[-b|x|\right]$ for $x < 0$.

| Reaction | $\sqrt{s}$ | Number n of charged particles | | | | | |
|---|---|---|---|---|---|---|---|
| | | All Prongs | 2 | 4 | 6 | 8 | 10 |
| $\pi^- p$ | 4.0 | - | 7.71 ± 0.24 | 7.60 ± 0.09 | 10.24 ± 0.19 | 11.17 ± 0.55 | - |
| $K^+ p$ | 4.8 | 10.6 ± 0.7 | - | - | - | - | - |
| $\pi^+ p$ | 6.0 | 10.29 ± 0.07 | - | 8.36 ± 0.10 | 10.89 ± 0.12 | 13.02 ± 0.23 | 14.24 ± 0.60 |
| $\pi^- p$ | 6.0 | 9.83 ± 0.08 | 8.82 ± 0.34 | 8.44 ± 0.10 | 10.32 ± 0.14 | 12.44 ± 0.26 | 14.30 ± 0.79 |
| $\pi^- p$ | 7.0 | - | - | 8.38 ± 0.62 | 10.43 ± 0.20 | 12.70 ± 0.27 | 15.34 ± 0.46 |
| pp | 6.0 | - | - | 7.29 ± 0.10 | 10.08 ± 0.20 | 12.80 ± 0.34 | - |

Table II

Values of a in the expression $dN/dQ = CQ^{3/2} \exp\left[-aQ\right]$

| Number of charged prongs | | a $(GeV/c)^{-1}$ | | |
|---|---|---|---|---|
| | | $\pi^- p$ | $\pi^+ p$ | $pp$ [a] |
| All | x > 0 | 6.75 ± 0.02 | 7.67 ± 0.03 | |
| | x < 0 | 7.86 ± 0.04 | 8.05 ± 0.05 | |
| 2 | x > 0 | 5.88 ± 0.05 | | |
| | x < 0 | 7.88 ± 0.18 | | |
| 4 | x > 0 | 6.61 ± 0.04 | 7.12 ± 0.04 | 7.77 ± 0.09 |
| | x < 0 | 7.49 ± 0.06 | 7.65 ± 0.06 | |
| 6 | x > 0 | 7.10 ± 0.05 | 7.68 ± 0.04 | 8.10 ± 0.11 |
| | x < 0 | 7.86 ± 0.06 | 8.05 ± 0.05 | |
| 8 | x > 0 | 7.74 ± 0.08 | 8.47 ± 0.08 | 8.85 ± 0.15 |
| | x < 0 | 8.45 ± 0.12 | 8.50 ± 0.09 | |
| 10 | x > 0 | 8.80 ± 0.27 | 9.66 ± 0.20 | |
| | x < 0 | 10.24 ± 0.29 | 10.56 ± 0.22 | |

could be achieved without a downstream spectrometer, since $\Delta p/p$ will be $< 10\%$ for all secondary momenta up to about 150 GeV/c. A comparable $(\Delta p/p)$ in the "bare" chamber is expected for a secondary momentum of about 25 GeV/c.

The equality of the values of b for $x < 0$ in different reactions might suggest scaling of $d\sigma/dx$; this would conflict with the Feynman hypothesis of scaling in $(2E/\pi\sqrt{s})$ $(d^2\sigma/dxdQ^2)$. However, when we compare the distributions for $(d\sigma/dxdQ^2)$ at 8 and 18.5 GeV/c with the distributions of $(2E/\pi\sqrt{s})$ $(d^2\sigma/dxdQ^2)$ at the same two energies (See Fig. 4) we find that the former distributions differ more, both in absolute value near $x = 0$ and in shape, than do the latter. This suggests that Feynman's hypothesis is more nearly correct even at the low energies now available. We do, however, still observe some difference in absolute magnitude for $f(x, Q, s)$ at 8 and 18.5 GeV/c. The corresponding distributions for $\pi^-$ from $\pi^+p$ at 18.5 GeV/c differ by a much greater amount. The values for $(2E/\pi\sqrt{s})$ $(d^2\sigma/dxdQ^2)$ are seen to differ by a larger amount at forward values of x. Thus it is important to test scaling in the region $x > 0$ at the highest possible incident momenta. The proposed experiment will enable a determination of the differential distribution out to larger values of positive x than can be obtained in the "bare" bubble chamber. Thus it will provide additional information on the validity of scaling and will allow a study of the effects of "leading" particles as a function of incident momentum.

A study of the distributions of variables such as the "rapidity" or "boost" variables suggested by Feynman[1] and DeTar[13] will be considerably aided by the availability of information on fast forward tracks provided by

the downstream spectrometer. These distributions are of interest since they may allow a distinction between fragmentation and multiperipheral models. If the multiperipheral models are valid, distributions of the rapidity variable $w = -\ln\left(\frac{E-p_{\parallel}}{\sqrt{Q^2 + m^2}}\right)$ are expected to exhibit a plateau at high incident energies. In contrast, the limiting fragmentation models would suggest a "two-peaked" distribution although "pionization" might modify this. At 18.5 GeV/c, rapidity distributions show a tendency to flatten near $w = 0$ (see Fig. 5) but this is not yet pronounced. While it will be possible to examine rapidity distributions throughout the range of w corresponding to negative x and "wee" x ($|x| < \frac{1\ \text{GeV/c}}{p_o}$) in the bare bubble chamber, a clear determination of the shape of the distributions near $x = 0$ can be more easily obtained if more of the distribution for $x > 0$ can be studied. This is especially important in view of the strong variation of w with Q near $x = 0$. In order to obtain good statistics it will be desirable to integrate over a wide range of Q. At an incident $\pi^-$ momentum of 300 GeV/c the possible c.m. values of w range from about -5.1 to + 5.1. A value of $w = +2.33$ is obtained for a secondary track with $p_{lab} = 18.2$ GeV/c when $Q = 0$. However, to be able to measure w values out to + 2.0 for all values of $Q < 1$ GeV/c requires a good determination for $p_{lab}$ for secondary tracks at momenta as large as 92 GeV/c.

C. Symmetry of Longitudinal-Momentum Distributions: Quark and Multiperipheral Models

The distributions of x observed at 8 and 18.5 GeV/c are generally found to be asymmetric (see Fig. 1), being more steep for $x < 0$ than for $x > 0$. The asymmetry is somewhat more pronounced for $\pi^-p$ interactions,

but is also evident for $\pi^+ p$, and was observed in $K^+ p$ interactions as well[8]. Thus, an interpretation of the entire asymmetry in terms of the simple "leading particle" picture in which the beam particle continues in the forward direction will not explain the data.

The asymmetry of the longitudinal-momentum distributions is dependent on the frame of reference, decreasing as one goes from the laboratory to the c.m. system. This suggests that a reference frame may exist in which the longitudinal-momentum distribution is symmetric about zero. A natural system for symmetry may follow from a given model for the interactions. For example, a simple quark-quark interaction model might suggest symmetry of the produced particles in the c.m. of the interacting quarks. The multiperipheral model, in contrast, where the interaction is schematically represented as

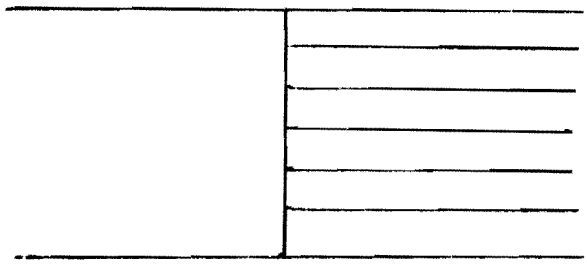

would suggest that, for particles produced far from the ends of the chain, symmetry might be expected in the overall c.m. of the interaction. The natural system for the fragmentation model would be the laboratory frame for the fragments of the target and the projectile frame for fragments of the incident particle.

To describe the system in which the $p_{//}$ distribution is symmetric,

we define a quantity $R = |p_t/p_{in}|$ where $p_t$ and $p_{in}$ are the momenta of the target and the incident particle. In Fig. 1c we show the value of R for which the x-distribution approaches symmetry as a function of n for $\pi^+p$ and $\pi^-p$ interactions at 18.5 GeV/c. The value of R decreases monotonically for increasing n in both $\pi^+p$ and $\pi^-p$ interactions, and approaches the value 1 for large n. This suggests the relevance of the c.m. system in describing high-multiplicity events and might favor interpretation of the data in terms of a multiperipheral model. The value of R for simple quark-quark interactions in $\pi p$ collisions would be 3/2. The observed dependence of R on n is hard to understand in terms of a simple quark-quark model. However, Erwin has suggested that the quark model can still explain the observations by including considerations of phase space available and/or of multiple quark scattering. If phase-space factors are important, the value of R for a given multiplicity shoulddepend on the incident momentum. In contrast, observation of $R \to 1$ for high multiplicities, independent of incident energy, would favor the multiperipheral model.

In order to determine the value of R for which the x-distribution approaches symmetry it is necessary to know the x-distribution for a considerable range of positive x. This is particularly true for $R > 1$, since some tracks with positive $p_{//}$ in the c.m. system are shifted to negative $p_{//}$ by the transformation. Thus, a study of the dependence of R on multiplicity at high energies requires the information provided by a downstream spectrometer such as that described in this proposal.

D. Fragmentation and/or Diffraction Dissociation of Incident and Target Particles

Processes in which one of the initial particles dissociates into several charged particles which have, as a group, the same quantum numbers as the initial particle are expected to be important not only for their contribution to "inclusive" reactions but also in their own right. These processes, corresponding to exchanges with the quantum numbers of the vacuum,are expected to provide the few individual "exclusive" channels which may still have significant cross sections at high energy. They were first discussed by Good and Walker[11] and, more recently, have been considered in light of their contribution to fragmentation[2]. An interesting aspect of the proposed experiment is the study of these fragmentation or diffraction dissociation processes at high energy. It should be possible, by utilizing the information from the hybrid system, to isolate samples corresponding to target fragmentation, beam fragmentation, or both where all the final-state particles are charged. This will be accomplished by selecting events in which both longitudinal and transverse components of visible momentum are conserved. The resolution of the proposed hybrid system is expected to be sufficient to allow elimination of the majority of events involving additional neutral particles. Since the invariant mass of systems formed via diffraction dissociation is typically near the minimum possible value and the momentum transfer involved is small it will then be possible to select samples corresponding to beam dissociation without target dissociation by choosing events in which only one slow track is observed in

the bubble chamber while several charged particles pass through the spectrometer. A trigger based on the presence of more than one fast charged particle is needed. Similarly, target fragmentation events will involve several relatively slow charged particles in the bubble chamber and only one fast track in the spectrometer spark chambers. Selection of this latter sample will necessitate a trigger which does not require the presence of several fast forward particles. While the study of target fragmentation may be possible in the "bare" bubble chamber, a study of projectile fragmentation is dependent on the precision of measurement for fast forward tracks furnished by the downstream spectrometer. At current accelerator energies, the production of light $N^*_{1/2}$ resonances[16, 17] is typically on the order of .1 to 1 mb. Cross sections for production of low-mass $\pi^+\pi^-\pi^-$ systems in $\pi^-p$ interactions are comparable. For example, at 18.5 GeV/c, the cross section for $\pi^-p \rightarrow pA$ (1000-1400 MeV) is .22 mb where A represents any $\pi^+\pi^-\pi^-$ system in the indicated mass region[18]. If vacuum exchange is responsible for these events, the cross section should still be appreciable at 300 GeV/c. Similarly, the limiting fragmentation model[2] predicts constant or slowly-varying cross sections for such processes as incident momentum increases. A measurement of cross sections for such "exclusive" reactions at high energies will provide valuable information about the nature of fragmentation.

Fragmentation of the incident pion in the inclusive reactions $\pi^\pm p \rightarrow \pi^-$ + anything may be of special interest in light of our observations

at 18.5 GeV/c. N. N. Biswas[19] has indicated the value of a plot of $M_t p_{\parallel}(t)$ versus $\mu_b p_{\parallel}(b)$ where $M_t$ and $\mu_b$ are the masses of target and beam particles, respectively, and $p_{\parallel}(t)$ and $p_{\parallel}(b)$ are the momentum of the "inclusive" particle in the target and beam rest frames respectively. He has shown that

$$\mu_b p_{\parallel}(b) + M_t p_{\parallel}(t) = \sqrt{s}\, p^*_{\parallel}$$

where $p^*_{\parallel}$ is the longitudinal momentum of the "inclusive" particle in the c.m. system. Particles with a given transverse momentum Q lie along definite curves in such a plot, and regions corresponding to equal volume in phase space can be easily constructed. On such a plot, particles coming from target fragmentation are expected to appear as points at small values of $M_t p_{\parallel}(t)$ while particles coming from beam fragmentation will appear at small values of $\mu_b p_{\parallel}(b)$. Tracks corresponding to "pionization", as well as some tracks from beam and target fragmentation, will appear at relatively small values of both $M_t p_{\parallel}(t)$ and $\mu_b p_{\parallel}(b)$. We have plotted our data for $\pi^-$ from both $\pi^- p$ and $\pi^+ p$ interactions at 18.5 GeV/c. The results are shown in Figs. 6 and 7. They suggest that beam fragmentation may be more important than target fragmentation in the production of $\pi^-$ mesons in $\pi^+ p$ interactions as well as $\pi^- p$ interactions. An investigation of this phenomenon at higher incident energies will be of interest. A comparison with $\pi^+ p$ interactions will be especially valuable, if a beam sufficiently enriched in $\pi^+$ mesons can be produced at high energies.

E. Distributions of Q and $Q^2$: Thermodynamic and Resonance Models

Distributions of the transverse momentum exhibit dependence on the multiplicity n and on x as illustrated in Fig. 2 which shows typical $Q^2$ distributions for 18.5 GeV/c $\pi^+p$ interactions. Data for $\pi^-p$ interactions exhibit similar features. An interesting feature of the distributions is the steep slopes at small $Q^2$ seen for all values of n when $|x|$ is small. The slopes at low $Q^2$ become less steep for larger $|x|$. The origin of these low-$Q^2$ peaks is not yet clearly established. Yen and Berger[20] have suggested that they are evidence for the importance of resonances in high-multiplicity events. The peripheral production and fore-aft decay of low-mass resonances could conceivably produce the observed low-$Q^2$ peaks. Such resonances should be more important for low-multiplicity final states and should be predominantly of the same charge as the initial particles. Thus peaks in $\pi^-$ distributions should be less prominent for $\pi^+p$ than for $\pi^-p$ interactions if meson resonances were responsible. However, at 18.5 GeV/c we observe peaks of approximately equal prominence for $\pi^+p$ and $\pi^-p$ interactions. If peripherally-produced low-mass baryon resonances are responsible, the effects might be the same in $\pi^+p$ and $\pi^-p$ data. A better test for the importance of resonances can be made by looking for similar effects in $\pi^-$ distributions at the higher incident momenta of the proposed experiment. It is kinematically possible at 18.5 GeV/c for $\pi^-$ from peripherally-produced low-Mass $N^{*+}$ decaying to $p\pi^+\pi^-$ to appear at x-values consistent with the observed low-$Q^2$ peaks. At higher incident energies, calculations based on the kinematics of such decays suggest that contributions from such a source will be greatly reduced and will be limited to smaller

values of x. A test of the resonance model appears to be possible with measurements made in the "bare" bubble chamber, but results of the proposed hybrid experiment will be useful in checking for the presence of low-$Q^2$ peaks at larger values of $x > 0$.

If the features of the transverse-momentum distributions are not explained by resonance production, they must somehow be explained by other means. The predictions of available models as to the detailed shapes expected for the Q-distributions are limited. Models such as the usual multiperipheral model predict the dominance of small Q at all x, but generally do not predict detailed shapes. Thermodynamic models[3], however, do provide predictions for Q-distributions, even though their validity seems limited to an average over all multiplicities. The models predict x-dependent Q-distributions, but require additional elaboration before they can predict the details of this x-dependence. In view of their ability to make predictions unavailable from other sources, a test of these predictions at high energies is of value.

In Fig. 8 are shown representative Q-distributions at 18.5 GeV/c for several ranges of x. These distributions show a shift in the position of the peak towards higher Q and a broadening of the peak with increasing $|x|$. These features correspond to the increase in slope of the $Q^2$ distributions at low $Q^2$ observed for increasing $|x|$ in Fig. 2b. We have tried fitting these distributions in terms of the thermodynamic model. The Q-distribution predicted by the simplest form of Hagedorn's thermodynamic model is

$$dN/dQ = kQ \left[\exp\ (E/T) - 1\right]^{-1} dx, \qquad (4)$$

where $$E = \left[Q^2 + (xp_o)^2 + m_\pi^2\right]^{1/2}.$$

The smooth curves in Fig. 8 show fits obtained by numerical integration over a range of x. We find that at 18.5 GeV/c the x-dependence of these Q-distributions for all n is described well by expression (4) with T = 118 MeV. For $K^+p$ interactions at 11.8 GeV/c, Lander[8] finds similar agreement with T ≈ 120 MeV. The model predicts that the parameter T should approach 160 MeV in the high-energy limit. To test this prediction and to determine whether the apparent agreement at low energy is significant we need to extend the measurements to higher incident momenta over large ranges of x.

With the proposed hybrid experiment, distributions of Q may be studied for a large range of positive x as well as for negative x. The downstream spectrometer combined with better instrumentation of the beam will also provide a considerable improvement in resolution for transverse momentum Q, for tracks with large $p_{lab}$, over that which can be obtained with the "bare" bubble chamber.

It will not be surprising if the simple form of the thermodynamic model described in equation (4) fails to fit the data. It will then be possible to test formulations of the thermodynamic model which attempt to account for the anisotropy of the interactions in the overall c.m. system by allowing

a distribution of decaying "fireballs" with varying longitudinal momenta with respect to the overall center of mass.

F. Distribution of Fast Forward $\pi^o$ Mesons

An additional feature planned for the spectrometer system proposed in Section IV is a converter for $\gamma$ rays from fast forward $\pi^o$ mesons. It should be possible, with measurements of the interaction vertex in the bubble chamber and of the $\gamma$-ray conversion point in the downstream spectrometer, to determine both the frequency and directional distribution of fast $\pi^o$ mesons. Elbert et al.[21] have measured the $\pi^o$ frequency distributions in 25 GeV/c $\pi^-$p interactions with limited statistics. Their results suggest a disagreement with predictions of the multiperipheral model. More precise measurements at higher energies will clearly be of value.

## REFERENCES FOR SECTION III


[1] R. P. Feynman, "Behavior of Hadron Collisions at Extreme Energies," talk given at the Third International Conference on High Energy Collisions, S.U.N.Y. Stony Brook, September 1969; Phys. Rev. Letters 23, 1415 (1969).

[2] J. Benecke, T. T. Chou, C. N. Yang, E. Yen, Phys. Rev. 188, 2159 (1969); T. T. Chou and C. N. Yang, Phys. Rev. Letters 25, 1072 (1970).

[3] R. Hagedorn, Supp. Nuovo Cimento III, 147 (1965). A summary of references to the thermodynamic model is given in R. Hagedorn, "Remarks on the Thermodynamic Model of Strong Interactions," CERN Report TH-1174 (1970). See also S. Frautschi, "A Statistical Bootstrap Model of Hadrons" Cal. Inst. of Technology Report CALT-68-286 (1970).

[4] D. Amati, A. Stanghellini, and S. Fubini, Nuovo Cimento 26, 896 (1962); L. Caneschi and A. Pignotti, Phys. Rev. Letters 22, 1219 (1969); N. F. Bali, L. S. Brown, R. D. Peccei, and A. Pignotti, Phys. Rev. Letters 25, 557 (1970); Chan Hong-Mo, C. S. Hsue, C. Quigg, and J. M. Wang, Phys. Rev. Letters 26, 672 (1971).

[5] Proceedings of the Colloquium on High Multiplicity Hadron Interactions, Ecole Polytechnique, Paris, May 13-15, 1970.

[6] V. P. Kenney, invited paper at the Washington APS Meeting, 1971; N. N. Biswas, N. M. Cason, V. P. Kenney, J. T. Powers, W. D. Shephard and D. W. Thomas, Phys. Rev. Letters (to be published).

[7] A. Erwin, "Multiparticle Production," Conference on Expectations for Particle Reactions at the New Accelerators, Madison, Wisc., 1970; J. W. Elbert, A. R. Erwin, S. Mikamo, D. Reeder, Y. Y. Chen,

W. D. Walker and A. Weinberg, Phys. Rev. Letters 20, 124 (1968); J. W. Elbert, A. R. Erwin, and W. D. Walker, to be published.

[8] W. Ko and R. L. Lander, to be published; R. L. Lander, private communication.

[9] D. B. Smith, R. J. Sprafka, and J. A. Anderson, Phys. Rev. Letters 23, 1064 (1969); E. W. Anderson, E. J. Bleser, G. B. Collins, T. Fujii, J. Menes, F. Turkot, R. A. Carrigan, R. M. Edelstein, N. C. Hien, T. J. McMahon, and I. Nadelhaft, Phys. Rev. Letters 19, 198 (1967); D. G. Crabb, J. L. Day, N. P. Johnson, P. Kalbaci, A. D. Krisch, M. T. Lin, M. L. Marshak, J. K. Randolph, P. Schmueser, A. L. Read, K. W. Edwards, J. G. Asbury, G. J. Marmer, and L. G. Ratner, Phys. Rev. D1, 645 (1971). Valuable, if limited, information on pp collisions at cosmic ray energies has been presented by the Echo Lake Collaboration, Phys. Rev. Letters 25, 1979 (1970) and 26, 728 (1971).

[10] An alternative definition, $x = 2p_{\parallel}/\sqrt{s}$, is equivalent in the high energy limit and differs only by a scale factor at lower energies.

[11] M. L. Good and W. D. Walker, Phys. Rev. 120, 1857 (1960).

[12] For details of what is possible with the "bare" 30-in. hydrogen bubble chamber at NAL, see the proposal submitted by N. N. Biswas, N. M. Cason, V. P. Kenney, W. D. Shephard, and D. W. Thomas, entitled "Study of Multipion Production in High Energy $\pi^-p$ Interactions at NAL."

[13] C. E. DeTar, Phys. Rev. D3, 128 (1971).

[14] D. Silverman and C. I. Tan, Phys. Rev. D3, 991 (1971).

[15] N. F. Bali, A. Pignotti, and D. Steele, Phys. Rev. D3, 1167 (1971).

[16] K. J. Foley, R. S. Jones, S. J. Lindenbaum, W. A. Love, S. Ozaki, E. D. Platner, C. A. Quarles, and E. H. Willen, Phys. Rev. Letters 19, 397 (1967).

[17] J. V. Allaby, F. Binon, A. N. Diddens, P. Duteil, A. Klovning, R. Meanier, J. P. Peigneux, E. J. Sacharidis, K. Schlüpmann, M. Spighel, J. P. Stroot, A. M. Thorndike, and A. M. Wetherell, Phys. Letters 28B, 229 (1968).

[18] P. H. Smith, "The Reaction $\pi^- p \rightarrow p\pi^+\pi^-\pi^-$ at 18.5 GeV/c," Ph.D. Thesis, University of Notre Dame, 1970 (unpublished).

[19] N. N. Biswas, Internal Report, High Energy Physics Program, University of Notre Dame, April, 1971 (unpublished).

[20] E. Yen and E. L. Berger, Phys. Rev. Letters 24, 695 (1970); E. L. Berger, private communication.

[21] J. W. Elbert, A. R. Erwin, W. D. Walker, and J. W. Waters, Nuclear Physics B19, 85 (1970).

## FIGURE CAPTIONS FOR SECTION III

Fig. 1. Distributions of the longitudinal-momentum scaling variable x at 18.5 GeV/c: (a) dN/dx for $\pi^+$p data for all-, 4-, 6-, 8-, and 10-prong events; (b) dN/dx for $\pi^-$p data for all-, 4-, 6-, 8-, and 10-prong events; (c) dependence of R (see text), a measure of the coordinate system in which the x-distributions approach symmetry, on prong number n for $\pi^+$p and $\pi^-$p data.

Fig. 2. Distributions of the transverse-momentum-squared, $Q^2$, for $\pi^+$p interactions at 18.5 GeV/c: (a) $dN/dQ^2$ distributions with $0.0 < x < 0.1$ for all-, 4-, 6-, 8-, and 10-prong events separately; (b) $dN/dQ^2$ distributions for 4-prong events with $-0.1 < x < 0.0$, $0.0 < x < 0.1$, $0.1 < x < 0.2$, and $0.2 < x < 0.5$.

Fig. 3. Dependence of fitted parameters a and b in 18.5 GeV/c $\pi^\pm$p interactions: (a) a as a function of n, (b) a as a function of x, (c) b as a function of n, and (d) b as a function of $Q^2$, for all $\pi^+$p data. The corresponding parameters for $\pi^-$p data are shown in (e) through (h).

Fig. 4. (a) Distribution of $(2E/\pi\sqrt{s})\,(d\sigma/dx)$ as a function of x for $\pi^-$ in 18.5 and 8 GeV/c $\pi^-$p interactions. (b) Ratio of $(2E/\pi\sqrt{s})\,(d\sigma/dx)$ at 18.5 and 8 GeV/c as a function of x. (c) Distribution of $d\sigma/dx$ as a function of x in 18.5 and 8 GeV/c $\pi^-$p interactions. (d) Ratio of $d\sigma/dx$ at 18.5 and 8 GeV/c as a function of x. The curves shown in (a) and (c) for the two momenta are shifted by a factor of 10. The error bars shown in (b) and (d) indicate typical statistical uncertainties.

Fig. 5. Distributions of the rapidity w in the c.m. system for $\pi^-$ in $\pi^-p$ interactions at 18.5 GeV/c for all-, 4-, 6-, and 8-prong events.

Fig. 6. Biswas plot of $M_t p_{11}$ (t) versus $\mu_b p_{11}$ (b) for $\pi^-$ mesons produced in $\pi^-p$ interactions at 18.5 GeV/c.

Fig. 7. Biswas plot of $M_t p_{11}$ (t) versus $\mu_b p_{11}$ (b) for $\pi^-$ mesons produced in $\pi^+p$ interactions at 18.5 GeV/c.

Fig. 8. Distributions of dN/dQ for $\pi^-$ in $\pi^+p$ interactions at 18.5 GeV/c for events with $0.00 < x < 0.04$, $0.04 < x < 0.10$, $0.10 < x < 0.20$, and $0.20 < x < 0.50$. The curves are described in the text.

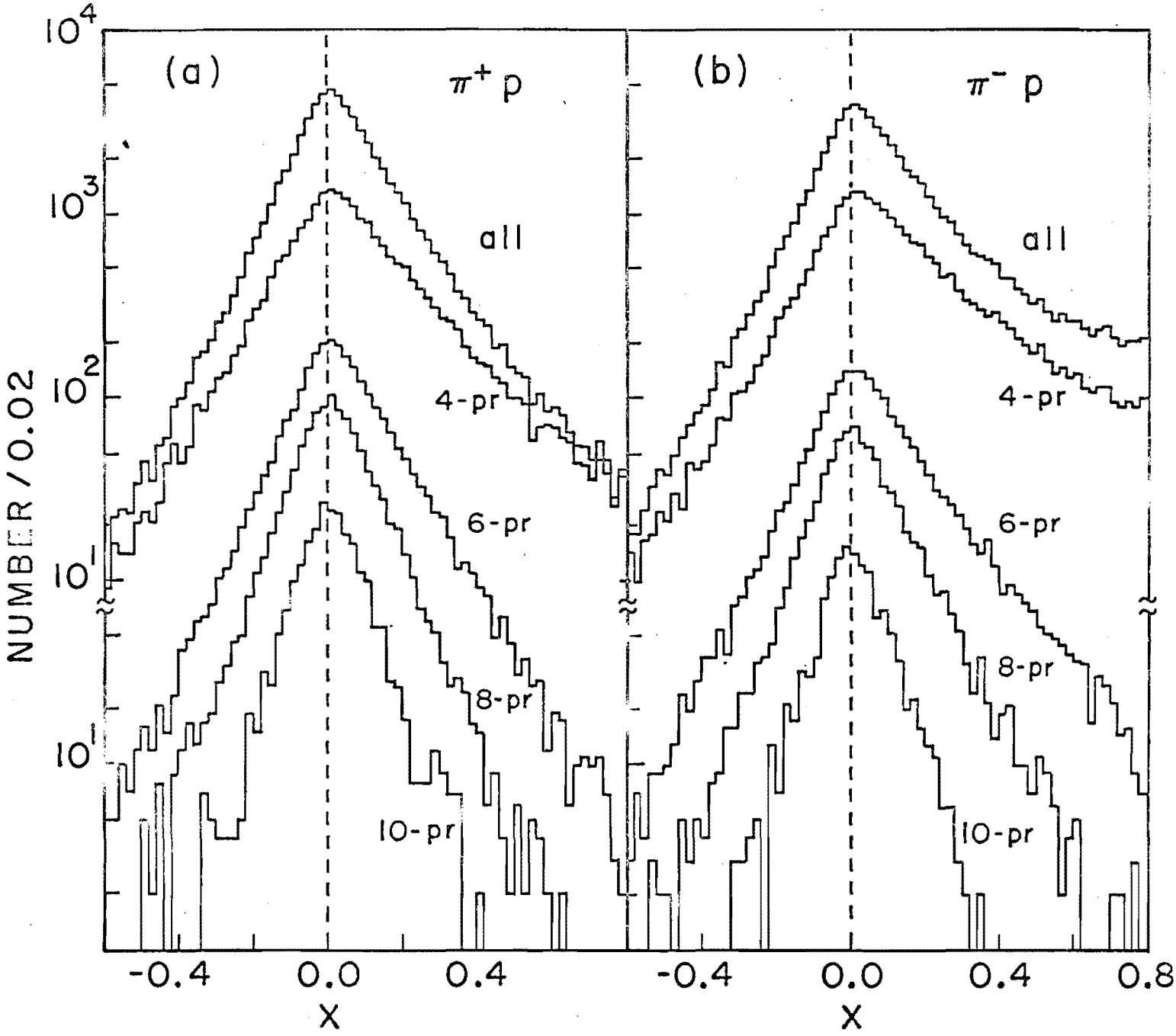
(a)
$\pi^+ p$
(b)
$\pi^- p$
all
4-pr
6-pr
8-pr
10-pr
NUMBER / 0.02
$10^4$
$10^3$
$10^2$
$10^1$
$10^1$
-0.4
0.0
0.4
0.8
X

Fig. 1

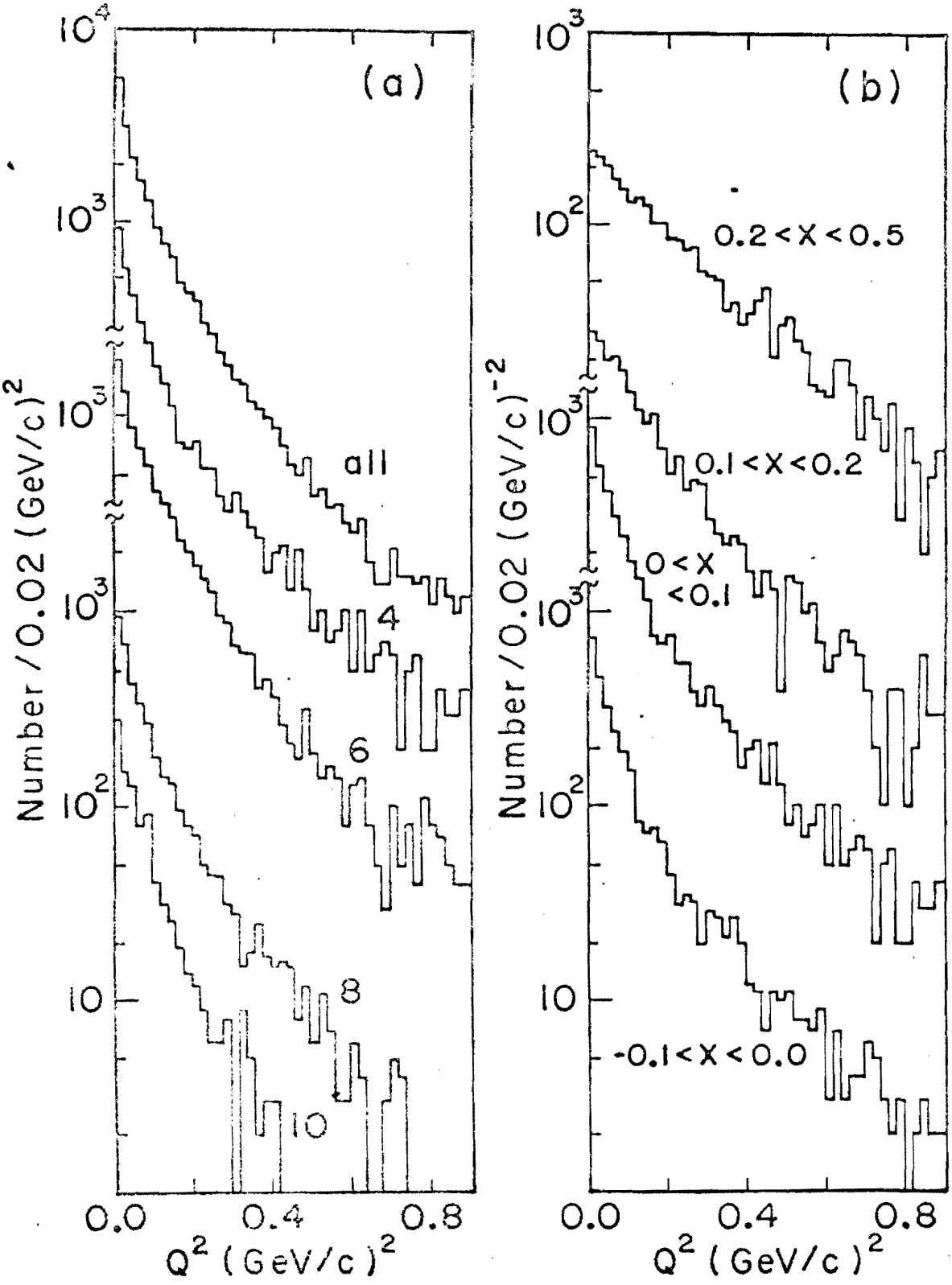
(a)
(b)
all
4
6
8
10
0.2<X<0.5
0.1<X<0.2
0<X<0.1
-0.1<X<0.0
Number /0.02 (GeV/c)$^2$
Number /0.02 (GeV/c)$^{-2}$
$Q^2$ (GeV/c)$^2$
0.0
0.4
0.8
10
$10^2$
$10^3$
$10^4$

Fig. 2

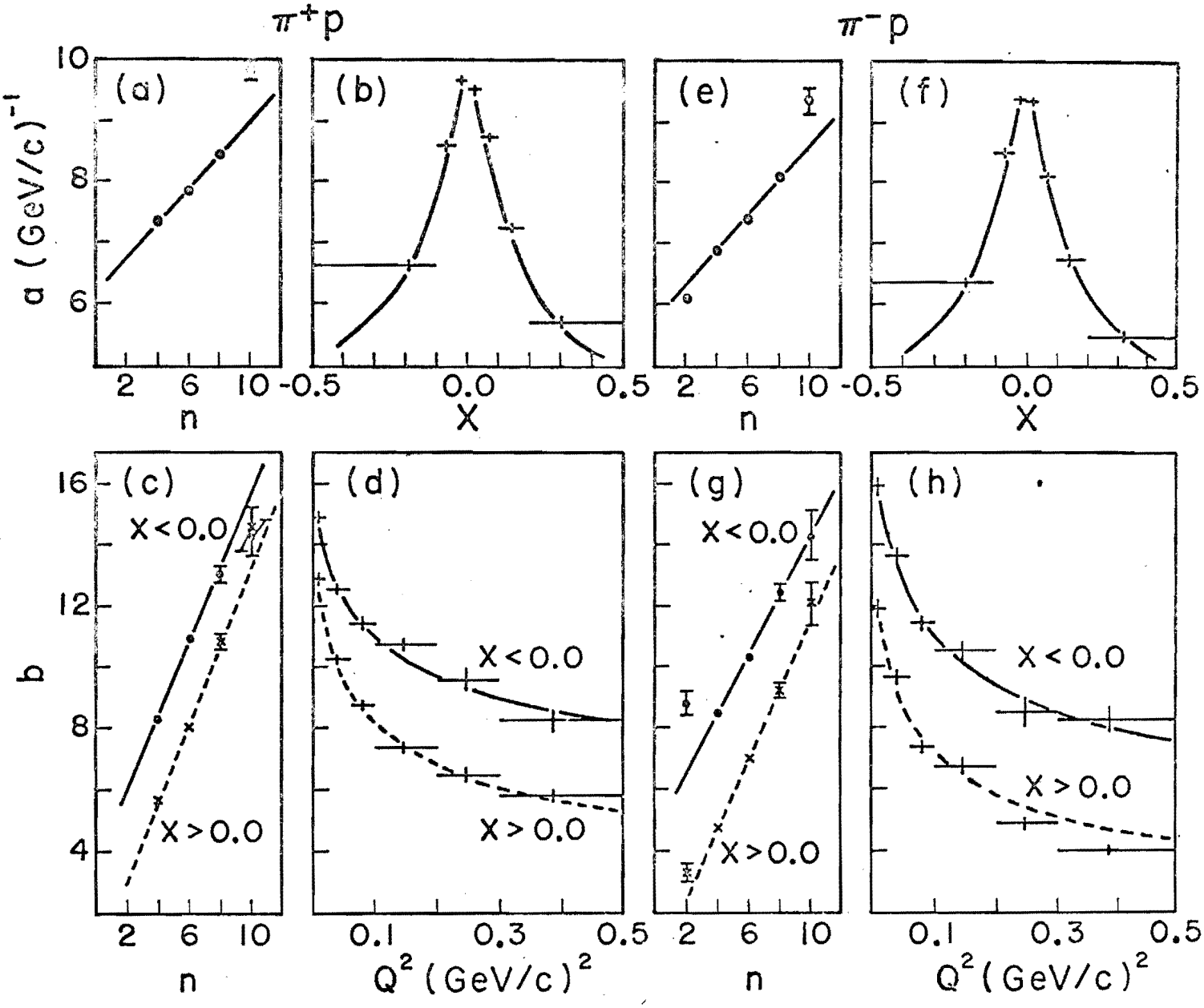


Fig. 3

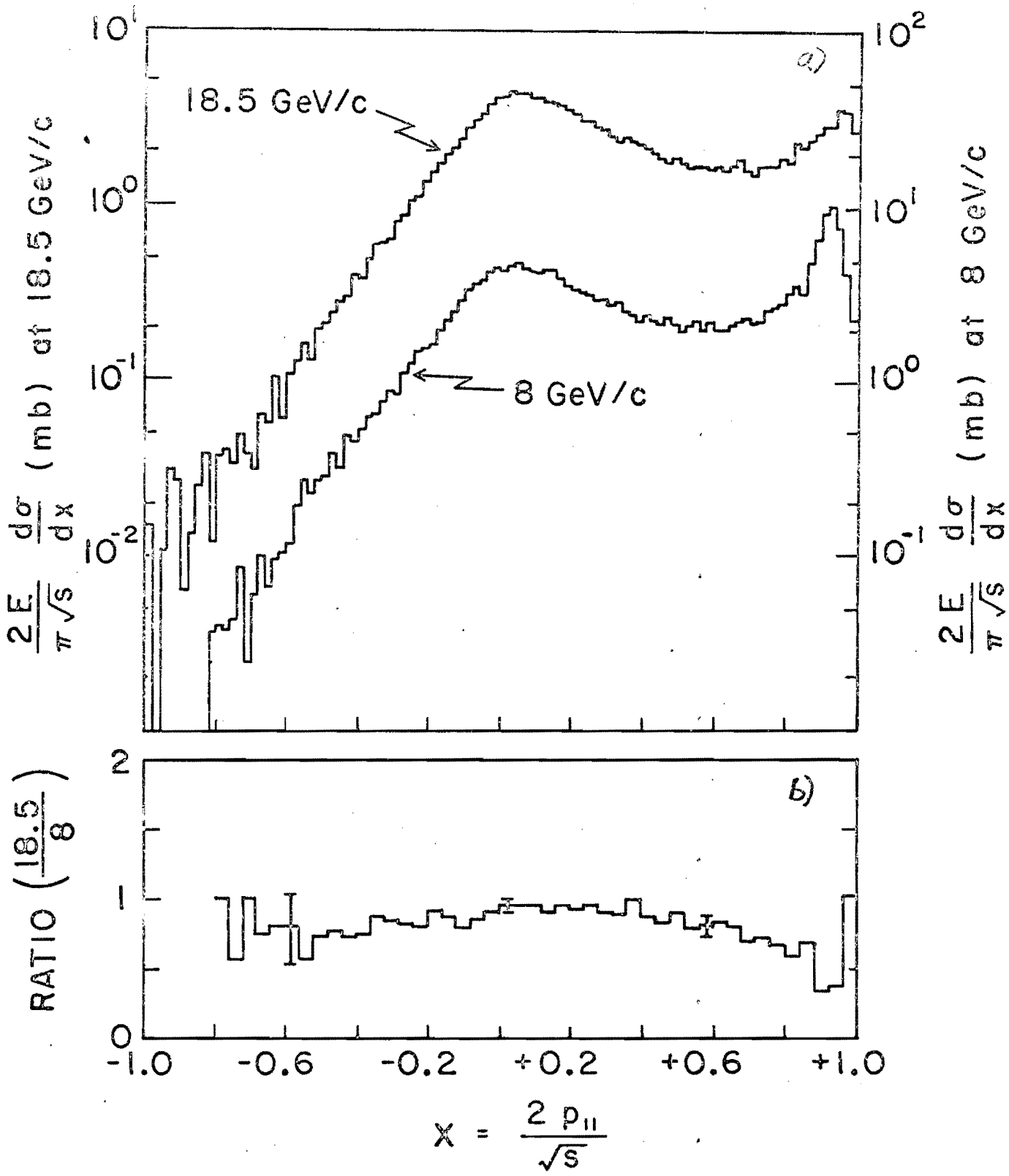
a)
18.5 GeV/c
8 GeV/c
$\frac{2E}{\pi\sqrt{s}}\frac{d\sigma}{dx}$ (mb) at 18.5 GeV/c
$\frac{2E}{\pi\sqrt{s}}\frac{d\sigma}{dx}$ (mb) at 8 GeV/c
b)
RATIO $\left(\frac{18.5}{8}\right)$
$X = \frac{2p_{\parallel}}{\sqrt{s}}$

Fig. 4

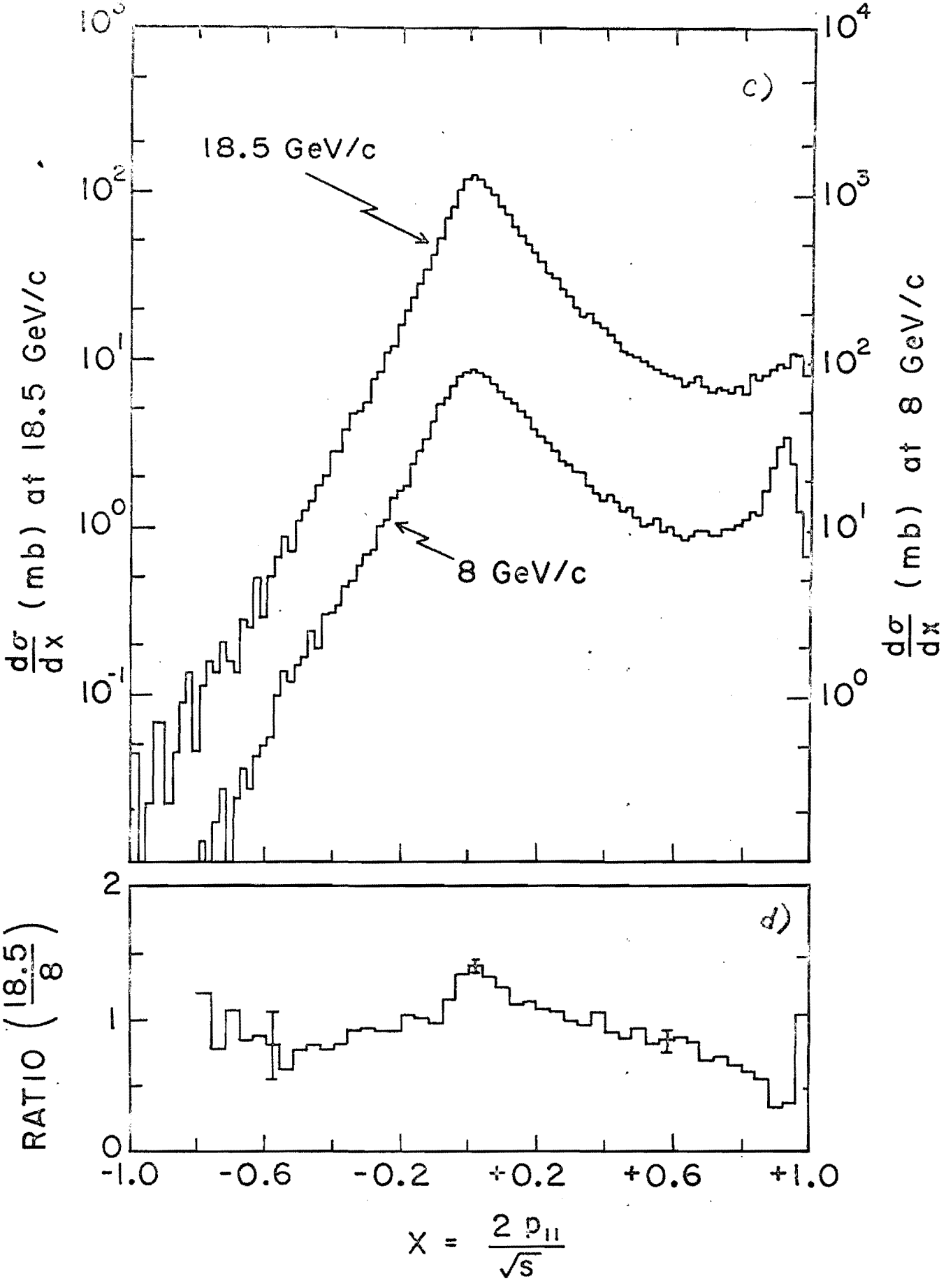
c)
18.5 GeV/c
8 GeV/c
$\frac{d\sigma}{dx}$ (mb) at 18.5 GeV/c
$\frac{d\sigma}{dx}$ (mb) at 8 GeV/c
$10^3$
$10^2$
$10^1$
$10^0$
$10^{-1}$
$10^4$
$10^3$
$10^2$
$10^1$
$10^0$
d)
RATIO $\left(\frac{18.5}{8}\right)$
2
1
0
-1.0
-0.6
-0.2
+0.2
+0.6
+1.0
$X = \frac{2 p_{11}}{\sqrt{s}}$

Fig. 4

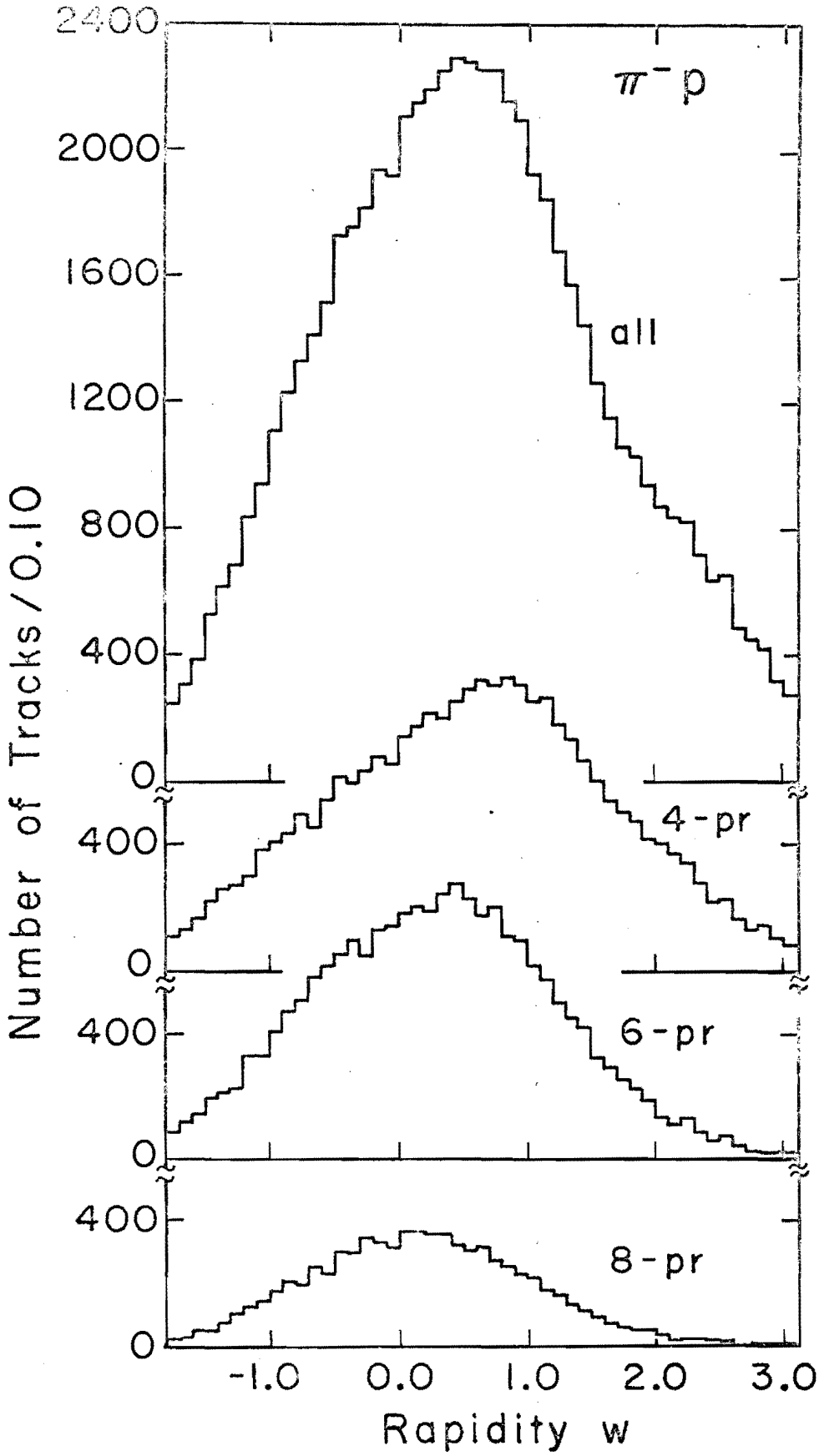
2400
2000
1600
1200
800
400
0
$\pi^- p$
all
400
0
4-pr
400
0
6-pr
400
0
8-pr
Number of Tracks / 0.10
-1.0
0.0
1.0
2.0
3.0
Rapidity w

Fig. 5

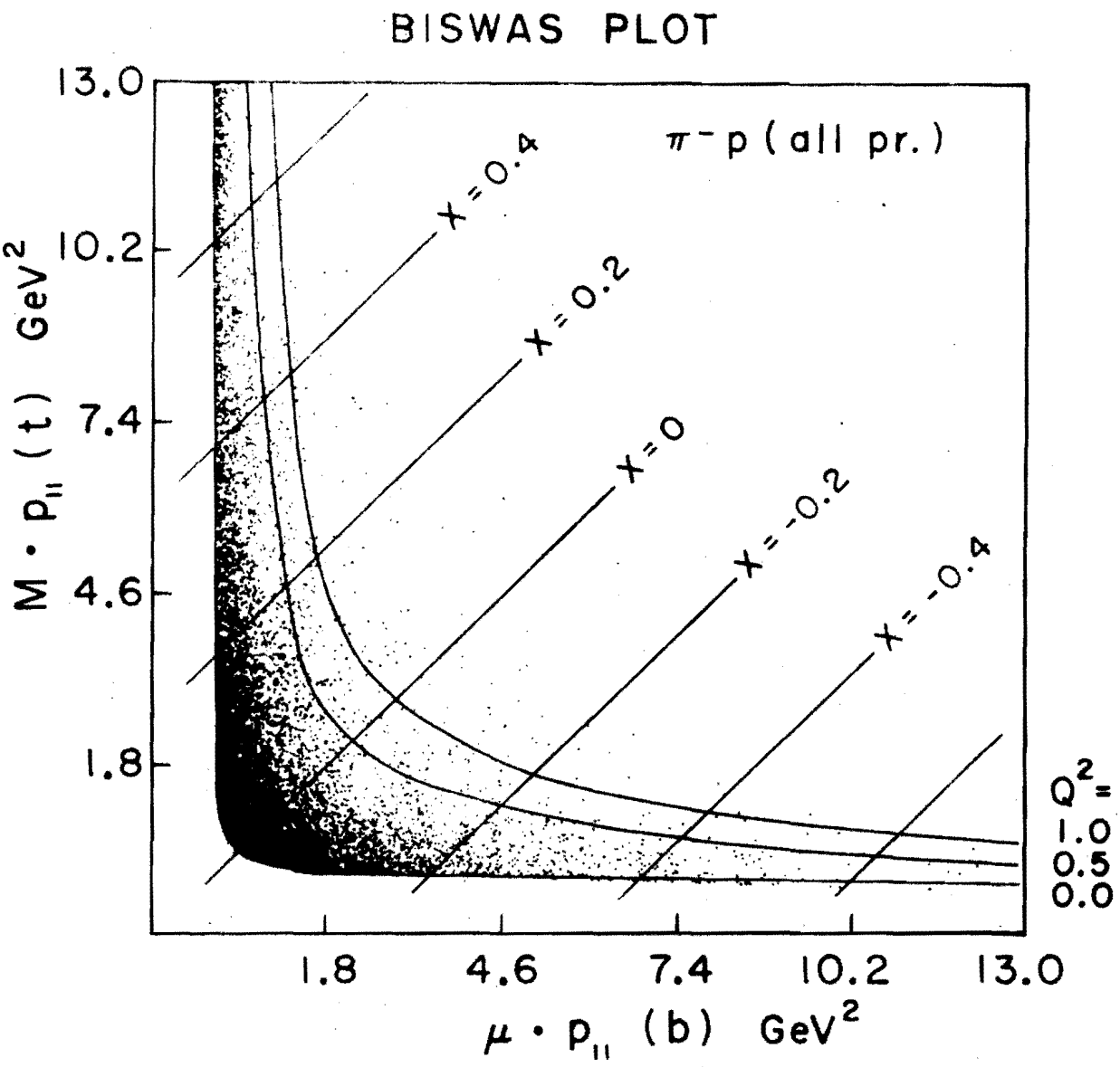
BISWAS PLOT
13.0
10.2
7.4
4.6
1.8
M • p11 (t) GeV2
π⁻ p (all pr.)
X=0.4
X=0.2
X=0
X=-0.2
X=-0.4
Q2=
1.0
0.5
0.0
1.8
4.6
7.4
10.2
13.0
μ • p11 (b) GeV2

Fig. 6

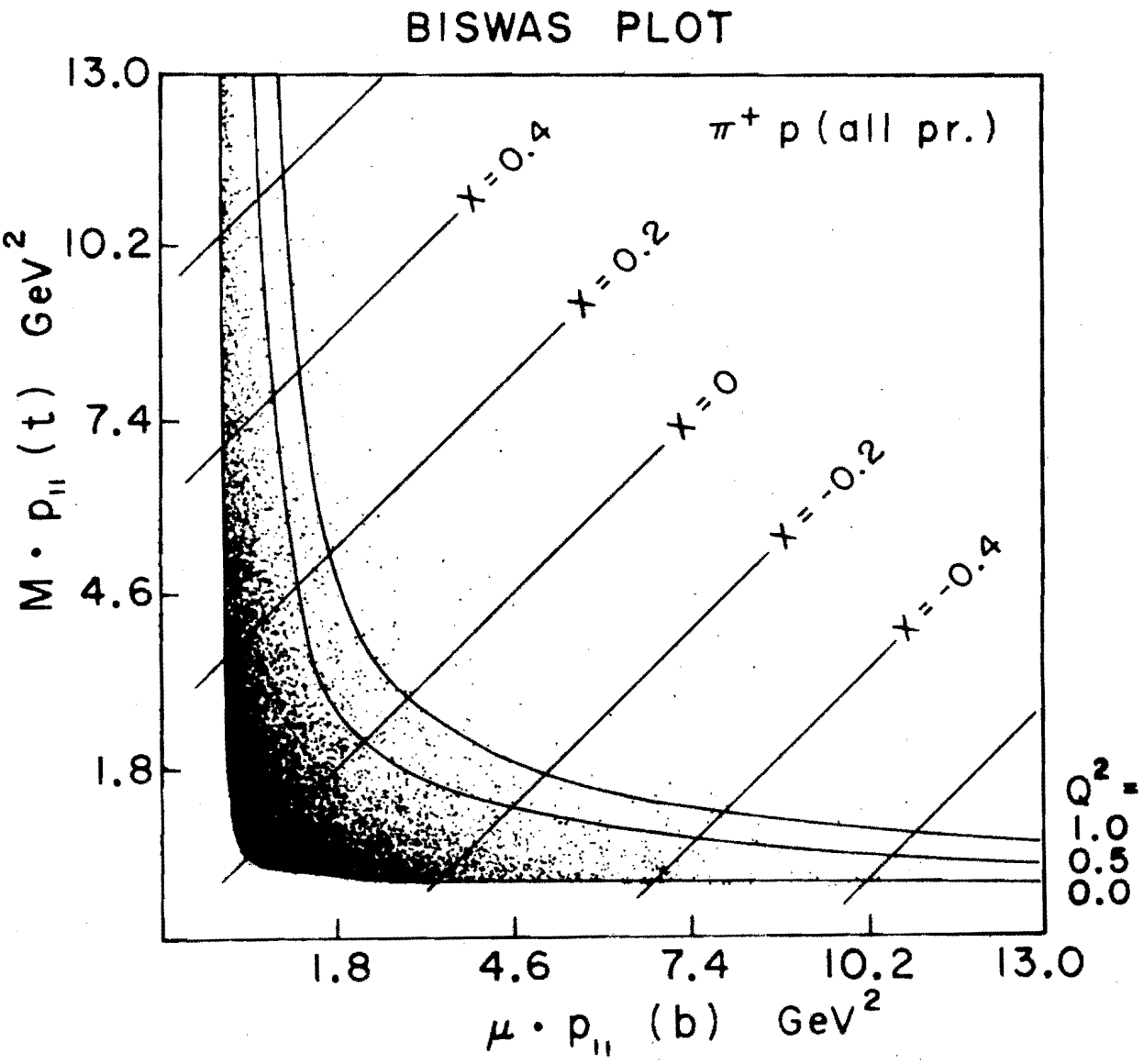
BISWAS PLOT
$\pi^+ p$ (all pr.)
13.0
10.2
7.4
4.6
1.8
$M \cdot p_{11}$ (t) GeV$^2$
X=0.4
X=0.2
X=0
X=-0.2
X=-0.4
$Q^2$ =
1.0
0.5
0.0
1.8
4.6
7.4
10.2
13.0
$\mu \cdot p_{11}$ (b) GeV$^2$

Fig. 7

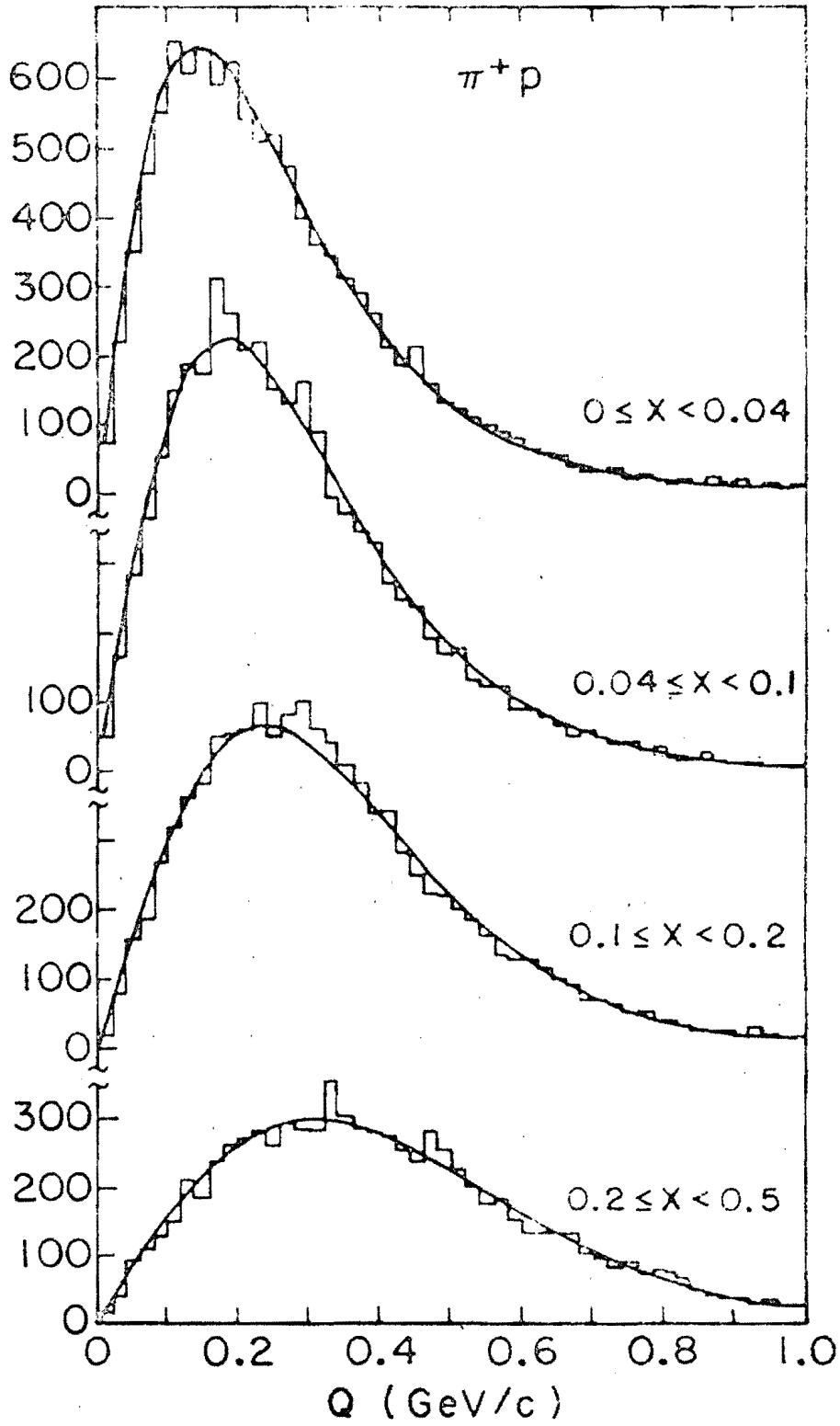
$\pi^+ p$
600
500
400
300
200
100
0
$0 \leq X < 0.04$
100
0
$0.04 \leq X < 0.1$
200
100
0
$0.1 \leq X < 0.2$
300
200
100
0
$0.2 \leq X < 0.5$
0
0.2
0.4
0.6
0.8
1.0
Q (GeV/c)

Fig. 8

# IV. Experimental Arrangement for the Proposed 30-inch Bubble Chamber - Optical Spark Chamber Hybrid System

The main components of the proposed detector system are shown in Figure 1. These include:

(1) The 30-inch hydrogen bubble chamber, for observation of the interaction vertex and analysis of all low energy charged particles with momenta below ~20 GeV/c.

(2) An upstream beam diagnostic system for providing precise measurements of beam particles.

(3) A wide gap optical spark chamber spectrometer situated downstream for providing important additional data on energetic secondary charged particles with momenta above approximately 20 GeV/c.

(4) A shower spark chamber system situated behind the spectrometer for information on very energetic gamma rays.

While the arrangement is similar in some respects to the bubble chamber - spark chamber detector system described in the Aspen study of Fields, et al.[1], it is not required for the present initial experiment to have the very high accuracy requirements for final state fitting which was of primary interest in the latter study.

These components are matched to the kinematic requirements, as discussed below, in such a way that they provide relatively complete examination of individual multiparticle interactions in the 100 GeV/c region and above. The most noticeable feature of multiparticle interactions as presently known is the tendency for the emitted particles to be produced with relatively small transverse momenta. Those going backwards in the cm system with large longi-

tudinal momenta then appear in the laboratory system with low momenta and large angles. Particles with small longitudinal momenta can appear in the lab at intermediate momenta and angles, while the forward particles in the cm appear as highly collimated, energetic components of a forward jet.

Examples of kinematically allowed regions for transverse and longitudinal cm momenta are shown in the Peyrou plot of Figure 2 for the case of 500 GeV/c pp interactions. Superposed are the expected contours for laboratory angles and momenta of outgoing pions, showing the characteristics described above. For greater detail, the region of small transverse momenta is shown in Figure 3. Backward pions in the cm with transverse momenta below 1 GeV/c are seen to have laboratory momenta of less than ~20 GeV/c, and can appear at angles even beyond 90°.

Similar behavior is illustrated for secondary protons from 200 GeV/c pp interactions in Figure 4, except that the allowed maximum laboratory angle here must be less than 90°. On the other hand, those particles produced with small or forward longitudinal momenta $P_L$, and transverse momenta $P_T \lesssim 1$ GeV/c, are seen to have laboratory momenta above approximately 20 GeV/c and are confined to a forward cone of less than approximately ±4° opening angle.

## A. Bubble Chamber

The main bubble chamber requirements here are good track resolution, angular precision $\lesssim 1$ mrad, good momentum accuracy up to the 20 GeV/c region, and provision of suitable exit windows and magnet apertures for the forward secondaries. The 30-inch bubble chamber is eminently suitable, without requiring any significant modifications.

The gross chamber features illustrated in Figure 1 are those of the 30-inch, whose characteristics include high resolution dark field optics, a

magnetic field of 32 Kg, multipulsing capabilities of $\leq$ five expansions per 0.5 seconds, and a maximum detectable momentum of over 1000 GeV/c. In the configuration shown in Figure 1, the beam is brought in through a small window which is currently in use as an exit window for a neutral hadron hybrid spectrometer at ANL. The limiting exit angle allowed by the magnet structure in the horizontal plane is confined to approximately ±3.5°, which corresponds to allowing all secondary particles above ~20 GeV/c to enter the downstream spark chamber spectrometer. In the vertical plane the magnet iron and beam exit windows allow particles at angles up to approximately ±10°. Thus, it is obvious that the analysis of tracks below ~20 GeV/c will necessarily be performed in the bubble chamber, where $\Delta p/p \leq 10\%$ and $\Delta\theta \leq 1$ mrad. This, in our opinion, is a satisfactory level of performance for this particular group of produced particles.

## B. Bubble Chamber Beam

Since the spectrometer facility is planned to be of general use, a comprehensive beam system is required. This section discusses beam characteristics and beam defining equipment which we regard as necessary to do a variety of experiments in the 30-inch bubble chamber with the associated downstream spectrometer. It is assumed that the beam, as described in the Lach-Pruss report[2], will be constructed, including a secondary hadron target. It is also assumed that fluxes of at least $10^{10}$ protons will be available at the secondary hadron target, with a spill time between 60 and 200 μ sec. Two or three such spills per accelerator pulse would be highly desirable for bubble chamber multi-pulsing. In addition, it is assumed that beam tuning detectors (scintillators or wire proportional chambers) will exist, and also at least one Cerenkov counter to determine relative fractions of π, K and p.

In addition,

A) it is felt that a flux-limiting fast kicker will permit much more efficient use of the bubble chamber, giving cleaner pictures and avoiding unusable pictures;

B) a Cerenkov counter which can efficiently tag $\pi$'s vs. (K and p) up to 200 GeV/c is desirable for beam purity in view of possible significant fractions of $K^-$ and $\bar{p}$[2,3];

C) a second Cerenkov counter which can tag ($\pi^-$, $K^-$) vs. $\bar{p}$ will permit studies of $K^-$ and $\bar{p}$ interactions as a by-product of a $\pi^-$ experiment. Eventually $K^-$ and $\bar{p}$ enrichment triggering might be done. If $K^+/p$ and $\pi^+/p$ ratios are good, similar arguments will apply for positive beams;

D) position tagging of each beam track in the chamber, in time correlation with the above Cerenkov signals, will be necessary.

E) external determination of beam momentum and angles will be mandatory in most cases. Five small proportional wire chambers can do this job and also tag all beam tracks in (D).

We now discuss items (A) - (E) in greater detail.

A) Fast Flux limiting Beam Kicker

A 1-2 $\mu$ sec. kicker with integral $Bdl \cong$ one Kg-m would kick the 5mm high target image upward by 0.065 mrad, or by 13 mm with a 200 meter lever arm. The kicker should be located 1000 feet from the chamber. However, the beam track counter should be placed at the chamber entry window to avoid uncertainty in n. The signal propagation delay ($\sim$2 $\mu$ sec.) is comparable to the rise time, plus there are logic and ignition delays. Given a total delay of 4 to 7 $\mu$ sec., n = 10 tracks/picture, and 100 $\mu$ sec. spill time, one could control the flux to 10%, which is excellent. This is enormously better than

the typical fluctuations without a kicker, and should eliminate a source of wasted bubble chamber photographs and wasted accelerator pulses.

B and C) Cerenkov Tagging of $\pi$, K and p

Extrapolations[3] of Serpukhov data indicate that 500 GeV/c protons on a target will produce a rich ratio of $K^-/\pi^-$ and $\bar{p}/\pi^-$ at 100 GeV/c -- 5% and 15% respectively, 1 km. away at the bubble chamber. The need for $\pi^-$ tagging in this case is obvious, and the opportunity to study tagged $K^-$ and $\bar{p}$ interactions early is attractive. In secondary positive beams, p and $\pi^+$ and probably $K^+$ will all be present in significant amounts at some energies, and will require tagging.

S. Pruss (NAL) has suggested a differential Cerenkov design, an outgrowth of ideas he presented at the 1970 Summer Study[4]. Small angle light is directed to one phototube and light between this angle and a larger angle is directed to a second phototube. For Cerenkov angles $\sim$5 mrad, the angular separation of $\pi$'s from K's at 200 GeV/c is several times the natural beam divergence of $10^{-4}$mrad, or the chromatic $\Delta\theta$. Good photon fluxes at these angles should permit efficient tagging at $p \lesssim$ 200-250 GeV/c or beyond. A second Cerenkov counter of identical design would then permit separation of p from K and $\pi$.

The design involves 40m of Helium-filled pipe at $\sim$.2 to 1 atmosphere absolute, downstream diameter 12" to 18", a 100" focal length spherical mirror, and the above-mentioned phototube array. High counting efficiencies can be obtained even beyond 200 GeV/c in the differential mode of operation with this length. Beam divergence must be $\lesssim$ 0.1 mrad, close to what is achievable in the existing beam design.[2] Pressure must be monitored to 10 mm of mercury and average temperatures to 5°C.

D) Position Tagging of Tracks to Correlate with Cerenkov Information

Minimal position tagging could be accomplished with a crossed pair of picket fence scintillator arrays. This means a non-negligible number of photomultiplier tubes, since the number, m, of x-y resolution elements should be many times greater than the number, n, of beam tracks to reduce the probability of two tracks in one hodoscope location. Moreover, one must record the bubble chamber frame number and x-y for each beam track. Thus, a fast parallel shift register is needed to absorb information during the beam spill and later pass it on to a computer or perhaps directly to an incremental tape unit.

With this in mind, we suggest the use of small proportional wire arrays of 50 to 100 wires, read out as above. One gets greater x-y resolution at somewhat less cost and can also achieve the purposes of item (E). Such a system is illustrated in Figure 5.

E) Angle and Momentum Tagging.

To use the 30" bubble chamber efficiently, one should start the fiducial volume immediately at the beginning of the liquid. Hence, one must know p and $\theta$ of the beam externally. In any case, one can do better externally than by measuring short beam tracks in the liquid. From beam optics one will have $\delta\theta \simeq 10^{-4}$ rad and $\delta p/p = 0.066\%$.[2] However, in flux-limited situations one may want to increase the momentum bite to 1%. Then it pays to replace the momentum slit with a proportional wire array and win back the $\delta p/p$ inherent in the target size. This corresponds to a wire spacing of 2mm. A more refined system can be made with 1 mm. wire spacing, but several such chambers would be required to determine orbits better. In effect, the equivalent of a second plane near the target is needed to reduce the "target size". In

this case one also improves upon the .066% which can be achieved with momentum slits.

The phase space of the beam as designed is $10^{-9}$ inch$^2$-steradian. With a reasonable beam size in the chamber, for example $\sim$ 0.5 x 3.0 inches, either the beam is parallel to $10^{-4}$ rad or its angle can be determined to $10^{-4}$ by measuring position in the chambers. This matches $\delta\theta_{coulomb} \lesssim 10^{-4}$ from the entry windows, and also matches for beam up to 500 GeV/c with the transverse momentum accuracy one obtains from measuring outgoing tracks in the last half of the bubble chamber or better still in the wide gap optical chambers.

To survey the proportional chambers, a well measured non-interacting track in the bubble chamber determines $\theta$ to $0.5 \times 10^{-4}$ in y, and $1.5 \times 10^{-4}$ in z, while $\delta\theta(\text{coulomb}) \sim 10^{-4}$ from the entry windows. At a distance of 13 m, the wire location is known to 1.5 and 2.4 mm respectively in y and z, from a single track.

We propose to use an existing, tested design of Charpak chamber[5] with good space resolution and immunity to spark chamber noise, compact and with a relatively small number of wires in total. We could certainly put the information onto magnetic tape, together with Cerenkov counter signals, for each beam track into the bubble chamber. Frame numbers would also be written onto the tape between beam pulses. A small computer would be the most flexible readout device. A fast parallel shift register or equivalent will be needed to interface the proportional wire and Cerenkov signals.

Notre Dame proposes to provide instrumentation to interface a small computer to the output of the proportional chambers and Cerenkov counter upstream from the bubble chamber and to provide the hardware and software necessary for magnetic tape output of the upstream beam information. A small computer and a magnetic tape unit can be provided for this purpose. Users of the hybrid spectrometer system who cannot conveniently use the resulting magnetic tape conveniently can then be provided with track tagging information printed out frame by frame for each roll if this is necessary. We believe this is the best way in which we can make a significant contribution to operation of the 30-in. chamber in a hybrid spectrometer mode at NAL. We have experience at Notre Dame with optical and wire spark chambers and have developed the hardware and software needed to output spark chamber and counter information on magnetic tape in previous experiments.

## C. Spark Chamber Spectrometer

Although many of the salient features of multiparticle interactions will be obtained from the analysis of only the low energy particles seen in the bubble chamber, as illustrated in the previous discussion, we believe that additional insight can be provided by supplementary information on the more energetic downstream components of the same events. The following deals with four important aspects of the system:

(A) spectrometer resolution,

(B) spark chamber optics,

(C) gamma-ray detection and,

(D) trigger schemes.

### (A) Spark Chamber Spectrometer Resolution

The apparatus, as shown in Figure 1, includes no external magnetic field other than that of the bubble chamber itself. Calculations show that utilizing (a) the event vertex location in the bubble chamber (b) the chamber's fringing field and (c) track locations in the wide gap chambers a typical $\Delta p/p$ accuracy of ±5-10% or less is readily obtainable for fast secondaries produced in a 200 GeV/c collision on hydrogen. It is clear, however, that considerable additional accuracy is available on the very small angle fast secondaries with the addition of a magnet downstream. Preliminary considerations for such a system are also presented.

In the initial scheme, two spark chamber units are utilized, one immediately behind the bubble chamber magnet with four gaps of active volume 36" wide by 48" high by 8" deep and the other unit 4.5 meters downstream, against

the far wall of the bubble chamber building, with the same dimensions. The downstream 36" dimension subtends a ±3.5° angle from the bubble chamber. Assuming the following perameters: (1) ±500 μ on each point measured in the spark chambers (2) eight points measured per spark chamber unit (3) ±50 μ on the vertex in the bubble chamber and (4) 872 Kg-in of integral Bdl in the bubble chamber fringing field we find that $\pm\Delta p/p$ (%) $\tilde{-}$ 0.07 p (GeV/c). Taking into account the following sources of error due to multiple coulomb scattering: (1) 15" of $LH_2$ (2) 0.12" of Fe (B.C. window) (3) 0.25" of Al (vacuum tank windows) and (4) 0.5 cm of counters and other smaller sources (air, chamber walls), the resultant $\pm\Delta p/p$(%) has been determined and is shown in Figure 6. With the exception of the fastest secondaries produced at the highest momenta proposed, the calculations show that the downstream spectrometer will provide data comparable in accuracy to that of the bubble chamber at lower secondary momenta and permit a complete study, in conjunction with the bubble chamber, of all interesting production angles.

The necessary and straight forward extension of the apparatus to yield more precision in the momentum determination of fast forward particles requires an additional spark chamber module plus a magnet. This would involve a large aperature magnet (e.g., an ANL type BM 109 with a 8" x 24" x 72" aperature and maximum integral Bdl of 1366 Kg-in) placed immediately downstream of the second spark chamber module followed by a third spark chamber module 5 meters from the magnet. All tracks with lab momentum $\gtrsim$ 100 GeV/c and with transverse momentum $\lesssim$ 1 GeV/c will be transmitted through the aperature of the magnet and will be recorded in the third spark chamber module. The deflection in the magnet, coupled with the long lever arm, provides a $\pm\Delta p/p \gtrsim .012\ p$ (%). Thus, 6-7% $\pm\Delta p/p$ or less can be achieved for all tracks of interest without altering the initial setup of the experiment.

(B) Spark Chamber Optics

The wide gap chambers have an active volume 8" deep x 48" high x 36" wide per cell. Each chamber consists of 2 cells and each module consists of 2 chambers, as seen in Figure 7. The chambers are mounted on a precision platform which has three primary functions: 1) Providing a means of determining the relative locations of the two chamber modules and the bubble chamber, 2) Providing a means of maintaining a continuous check on these positions and 3) Providing a simple means of re-installing the apparatus in the beam line after removal. Measuring of apparatus locations is done by means of two theadolites, one to determine and monitor bubble chamber-spark chamber platform positions and the second to determine and monitor spark chamber-spark chamber platform positions. Leveling legs on the chambers, top, bottom, front, and rear fiducials on the chamber frame and fiducials on the precision platform serve to position the chambers in a known orientation. Front and top fiducials also appear on each film frame to orient the chambers on the film. Rear and bottom fiducials on periodically run fiducial runs serve to complete a three dimensional co-ordinate system for track reconstruction independent of knowledge of camera position. Additional platform fiducials in view of the camera can serve as an extra check on spark chamber-platform orientations.

The chamber separation is variable within and between modules. Within the module a maximum separation of 32" is allowed. As seen in Figure 8, this maximum separation still permits viewing both chambers in a module with one 35 mm. camera at a demagnification of 64:1. This demagnification is an upper limit permitted by the intrinsic resolution of a film such as Kodak Shellburst for a real space position accuracy of 0.1 mm. With a 4" lens

the camera can be located at 20 ft. from the center of the chambers. The chambers are inclined 6° relative to the beam line to permit a direct view in each chamber, thereby eliminating lenses and mirrors in that view (see Figure 9). The chamber windows are made of 10 mil. clear Mylar to eliminate distortions there. One precision mirror is used in the 90° stereo view to bring that view to the same camera. A fiducial plane with many fiducials is located at the bottom of the spark chamber to permit corrections due to any distortions in the mirror. 90° stereo is used for maximum accuracy in reconstruction. The direct view is the view of the plane of bend for maximum accuracy in momentum determination. A strip mirror subtending $\sim$ 1/3 of the gap in the direct view provides 10° stereo for resolving ambiguities in track reconstruction. The mirror subtends only part of one gap in each chamber to eliminate confusion between the direct and 10° stereo tracks. A dark room under slight over pressure surrounds each assembly for photographic and hydrogen safety reasons.

(C) Gamma-Ray Detection

The insertion of several radiation lengths of material between the second and third gaps of the spark chamber units will provide an effective converter for gamma-rays from fast, forward $\pi^\circ$'s. From the point of interaction, probably measureable to $\lesssim$ 5 mm, both the frequency and direction of fast $\pi^\circ$'s can be inferred. To our knowledge, the only previous measurement of $\pi^\circ$ frequency is that of Elbert et al.[6] at 25 GeV/c for $\pi^- p$ in a hydrogen bubble chamber with plates. Their results, although somewhat weak statistically, are in rather strong disagreement with the multiperipheral model. Clearly, more precise measurements at NAL energies will be very valuable in our proposed studies.

(D) Trigger Schemes

The trigger arrangement will be designed such that the spark chambers fire on virtually all interactions, there being nearly one per beam burst. A picture of the bubble chamber will be taken for each expansion. Two simple and flexible schemes have been devised:

(1) Energy-Loss Trigger: Referring to Figure 1, multiparticle-charge-particle secondaries would be selected by pulse-height criteria in the counters $S_3$ $S_4$ $S_5$. More than one particle will, on the average, give a greater pulse height than that for a single beam particle. Although one might consider almost any type of counter which gives signals proportional to the number of particles which transverse it, e.g. Cerenkov, scintillation, etc., the most simple to utilize is the scintillation counter and it also turns out to result in the thinnest detector (in $g/cm^2$). A single scintillation counter when traversed by a high energy particle will give a Landau pulse-height distribution. This distribution, with its long tail at high pulse heights, cannot be avoided in the present application. A pulse height of 2 times the minimum value will occur on traversal by a single minimum ionizing particle ~5% of the time. This can be greatly improved, however, if two or more counters $S_1$, $S_2$; $S_3$ $S_4$...$S_n$ are utilized and the minimum pulse height appearing is considered. In this case, the width of the distribution will be decreased by $1/\sqrt{n}$ and even for n = 3, the tail has all but vanished. If this signal is to be used to trigger the downstream chambers, the minimum pulse height must be determined in $<<1$ $\mu$ sec.

With this method, it is to be noted that the downstream counters should be thin in order that nuclear interactions in them do not occur frequently. Such interactions are no different in character from those in the chamber and

walls and triggers due to them would certainly result. The number of these should be much smaller than those which occur in the chamber. In 1 mm of plastic scintillator a minimum ionizing particle produces $\sim 10^3$ photons. With an efficient photo cathode ($\sim$25%) and a light collection efficiency of $\sim$20%, 50 photo-electrons could result. This number is sufficient to assure that statistical fluxtuations will be relatively small. The five counters, $S_1$, $S_2$, $S_3$, $S_4$, and $S_5$, would represent a total thickness of 0.5 cm which is 0.5cm/52cm = 1/100 of a geometrical-mean-free-path. Thus, with 6 particles per picture and with the counters described, in $\sim$ 6% of the pulses would the spark chamber system have recorded interactions occuring in the triggering counters $S_1S_2S_3S_4$and $S_5$.

For reasons of efficient and uniform light collection the size of these counters probably should not exceed 8" x 8". This presents some minor limitations in the detection of secondaries as they must appear within a cone of $\pm 3°$ if placed at a distance of $\sim$2 meters from the interaction. It may be possible to locate counters nearer the chamber inside the iron yoke, and if so the acceptance angle would be increased. This setup is very inefficient for elastic scattering and processes of the type $pp \rightarrow ppn(\pi°)$, when the struck proton is slow and at a large angle, thus missing $S_3S_4S_5$. However, an alternate scheme, discussed next, would resolve this shortcoming. Also, with this arrangment one also might consider triggering on events with no charged secondary within the angular acceptance of $S_3S_4$and $S_5$. This alternate trigger could be tried with parallel logic and could be easily included or not as a parallel trigger.

(2) Beam-Deflection Trigger: The trigger consists of a 3.0 inch diameter scintillator $S_3$ located in the beam 125 feet downstream from the

bubble chamber (see Figure 1). When this scintillator fails to record a particle previously observed by counters $S_1$, $S_2$ in the beam upstream of the bubble chamber, it is considered to have interacted.

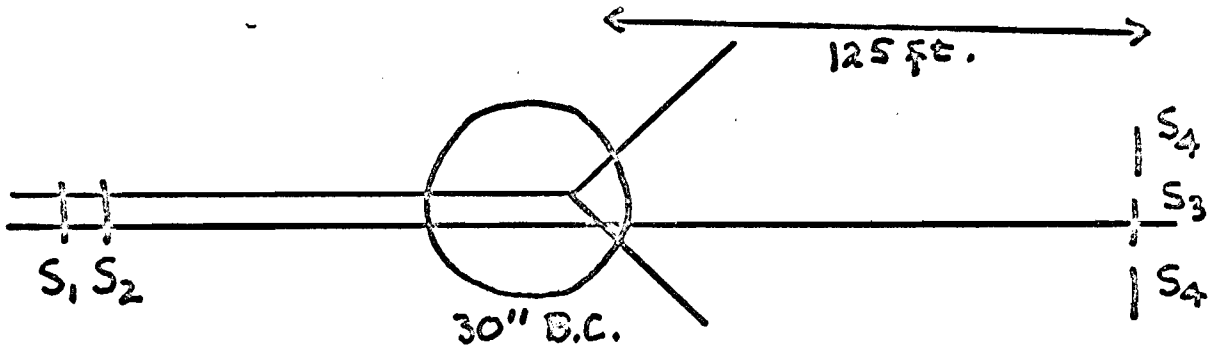


For the purposes of investigating the properties of the trigger we assume a 2.0" diameter beam in the bubble chamber. This allows a beam spread which does not diverge after leaving the chamber except for multiple Coulomb scattering. For beam momenta between 100 and 500 GeV/c the beam size at the downstream scintillator should not exceed 2.25 inches due to multiple scattering.

This trigger fails most frequently in detecting elastic scatters. Table II below lists the average minimum scatter angle and recoil range for elastic events which will actuate the trigger.

TABLE II - Minimum Angle and Recoil Range For Elastic Events

| Beam Momentum GeV/c | Minimum Scatter Angle mr. | Minimum Recoil Range cm |
|---|---|---|
| 100 | 1 | 0.3 |
| 200 | 1 | 3.5 |
| 300 | 1 | 15.0 |
| 500 | 1 | 100 |

There is considerable flexibility here. For example, by moving $S_3$ to 200 feet downstream of the bubble chamber and using a diameter of 2.5"

instead of 3.0", one achieves a minimum angle of 0.5 mr. and a minimum range of 8.0 cm at 500 GeV/c.

Some fraction of the inelastic events might also be expected to put a particle through $S_3$, invalidating the trigger. Scaling 25 GeV/c events to NAL energies indicates this is not very important, in part because the bubble chamber field imparts transverse momentum to a track which is several times that of the minimum detectable elastic scatter. For example at 200 GeV/c this trigger fails on 4.5% of the 2-prongs, 3% of the 4-prongs, 1% of the 6-prongs and 0.3% of the 8-prongs.

This small loss of inelastic events can be reduced somewhat by surrounding $S_3$ with a larger counter $S_4$. A hole in $S_4$ passes beam particles on to $S_3$. A multiparticle accidental through $S_3$ is likely to be accompanied by one or more particles through $S_4$. Hence one would trigger on $(S_1.S_2.\overline{S_3}.S_4)$, $(S_1.S_2.\overline{S_3}.\overline{S_4})$, $(S_1.S_2.S_3.S_4)$. One can reduce the loss rate arbitrarily by increasing the size of $S_4$ or moving it closer to the bubble chamber.

$S_3$ was not placed more than 125 feet downstream of the bubble chamber so that transit time of the particles and signals would be short enough to allow adequate time to perform logical operations and apply spark chamber voltages in less than 500 ns. This restriction is probably too strict by at least a factor of two and can probably be relaxed to observe smaller angle elastic scatters. Some groups will probably prefer a beam profile in the chamber more like 5" x 1/2". In this case $S_3$ would be about 6.5" x 1". This has approximately the same solid angle as the circular counter discussed above and presents no focusing problems for the presently planned beam.

Finally, it is emphasized that both these triggers are flexible and most certainly can be studied quickly and efficiently under test beam condi-

tions. It would be our intention to do so before proceeding with "production" data-taking.

## REFERENCES FOR SECTION IV


1. T. H. Fields, et al., NAL Summer Study, Vol. 3, 227 (1968).
2. "Hadron Beams in the Neutrino Area", J. Lach and S. Pruss, NAL Report TM-285, 2254.000.
3. "Extrapolated Ratios of $K^-$ and $\bar{p}$ to $\pi^-$ from High Energy Protons on Aluminum measured at Serpukhov," V. E. Barnes, Purdue University High Energy Physics Note # 313, April 1, 1971.
4. S. Pruss, NAL Summer Study (1970) p. 103.
5. M. Atac and J. Lach, Nucl. Instr. & Methods 86, (1970) p. 173.
6. J. W. Elbert et al., Nuclear Physics B19, 85 (1970).

## FIGURE CAPTIONS FOR SECTION IV

Fig. 1 Components of the proposed hybrid system.

Fig. 2 Contours of laboratory angle and momentum on the Peyrou Plot for the $\pi$ in the reaction $p + p \rightarrow \pi^+ + \ldots$ at 500 GeV/c.

Fig. 3 Shows more detail of Fig. 2.

Fig. 4 Detail of contours of laboratory angle and momentum on the Peyrou Plot for the proton in the reaction $p + p \rightarrow p + \ldots$ at 200 GeV/c.

Fig. 5 Upstream proportional wire spectrometer.

Fig. 6 Calculated momentum resolution for the apparatus of Fig. 1.

Fig. 7 Wide gap optical spark chamber (one of two such chambers).

Fig. 8 Wide gap optical spark chambers and camera positioning.

Fig. 9 Format of images on 35 mm film.

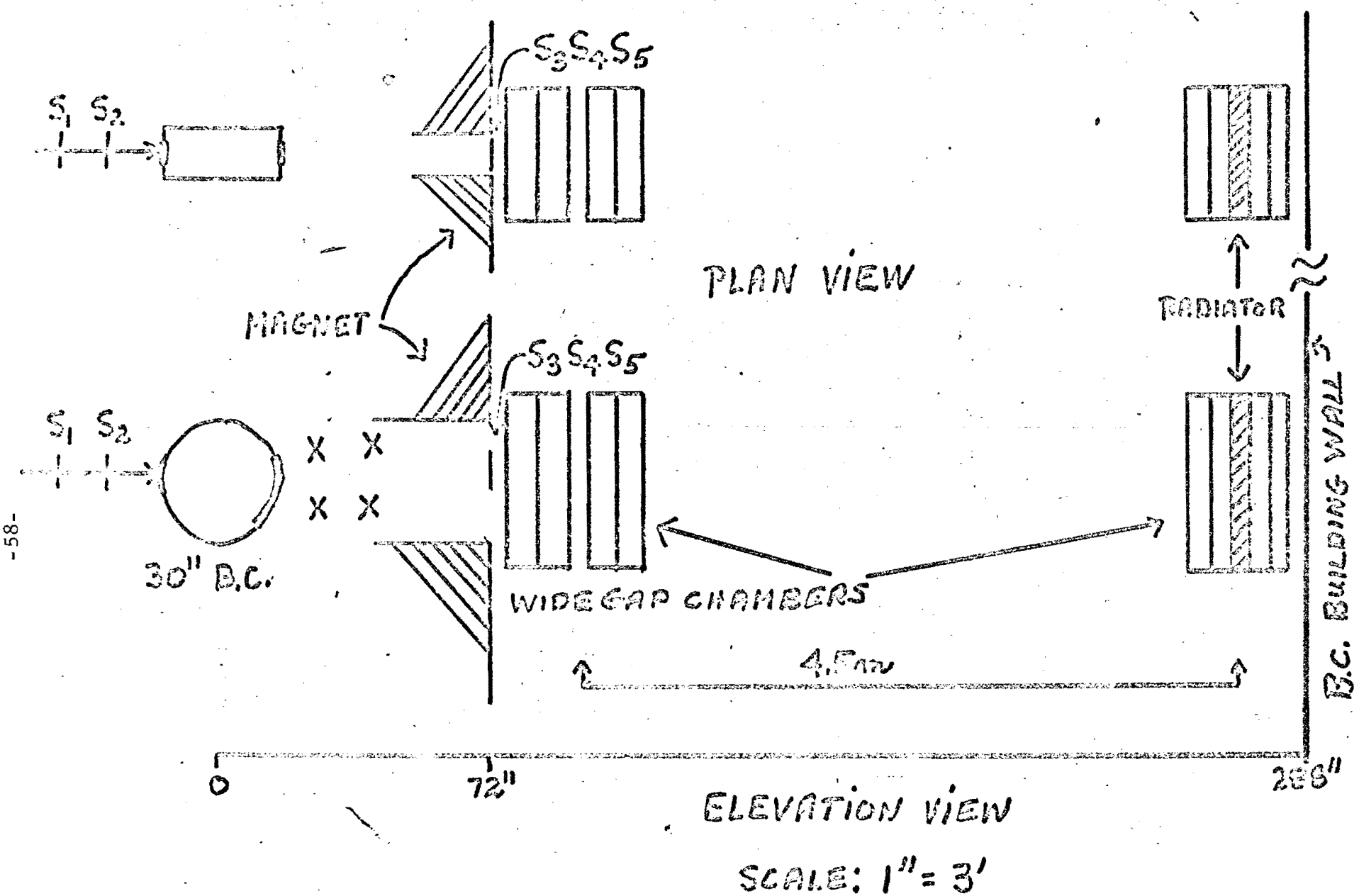
$S_1$ $S_2$
$S_3S_4S_5$
PLAN VIEW
MAGNET
RADIATOR
B.C. BUILDING WALL
30" B.C.
WIDE GAP CHAMBERS
4.5m
0
72"
286"
ELEVATION VIEW
SCALE: 1" = 3'

FIGURE 1

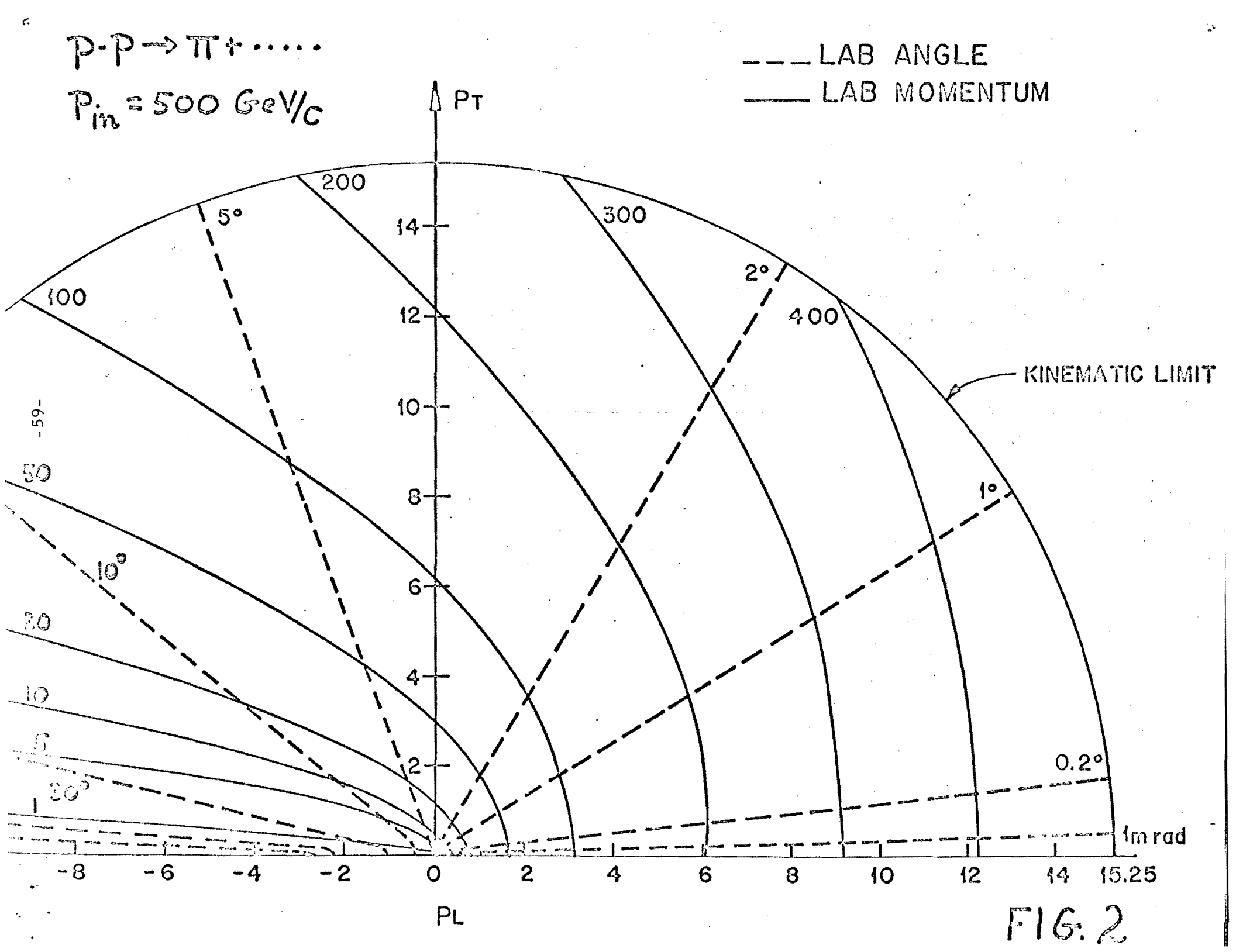
p-p → π+ .....
P_in = 500 GeV/c
--- LAB ANGLE
—— LAB MOMENTUM
PT
PL
KINEMATIC LIMIT
100
200
300
400
5°
2°
1°
0.2°
1m rad
50
10°
30
10
5
30°
1
14
12
10
8
6
4
2
-8
-6
-4
-2
0
2
4
6
8
10
12
14
15.25



FIG. 2

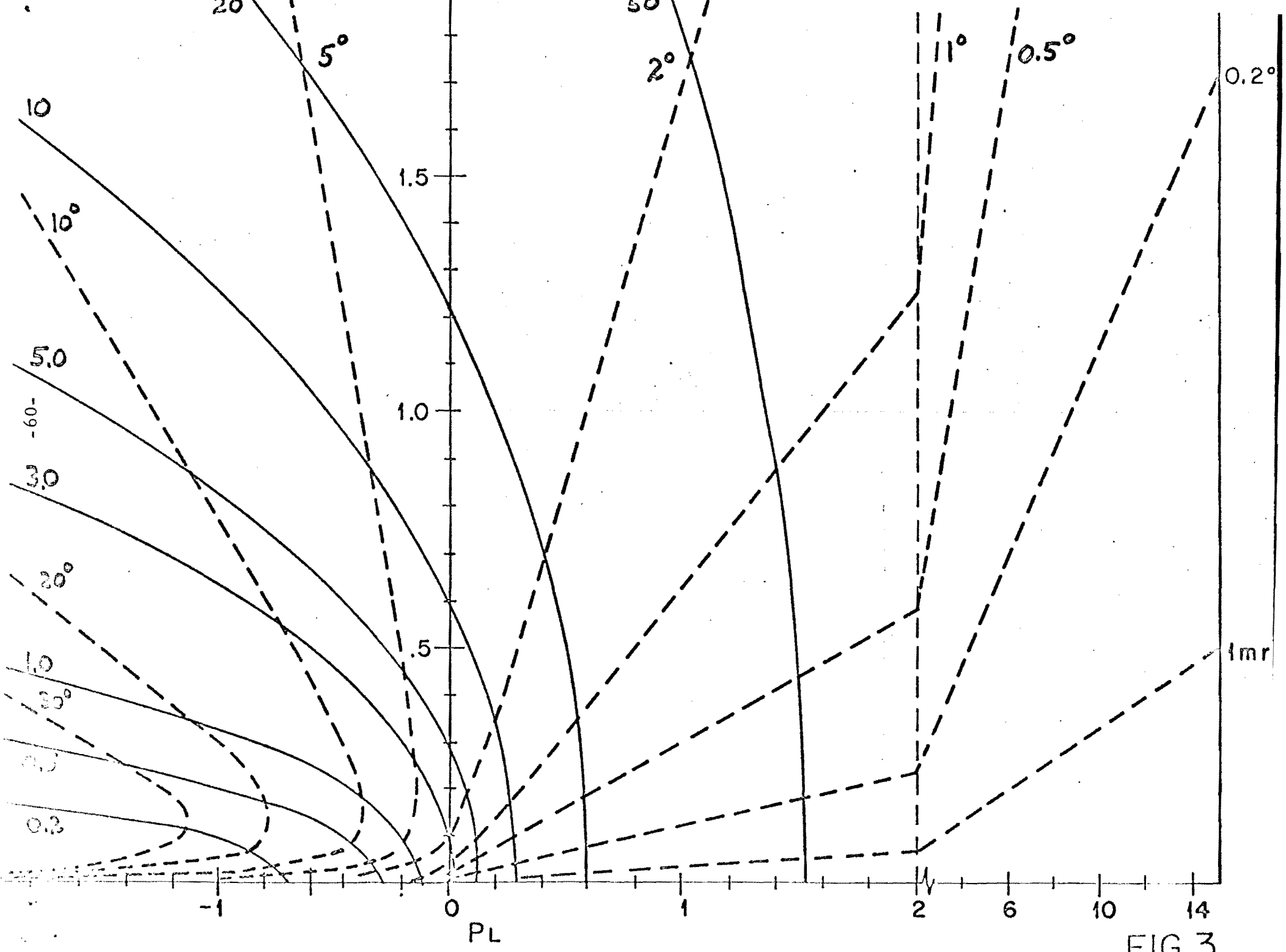


FIG. 3

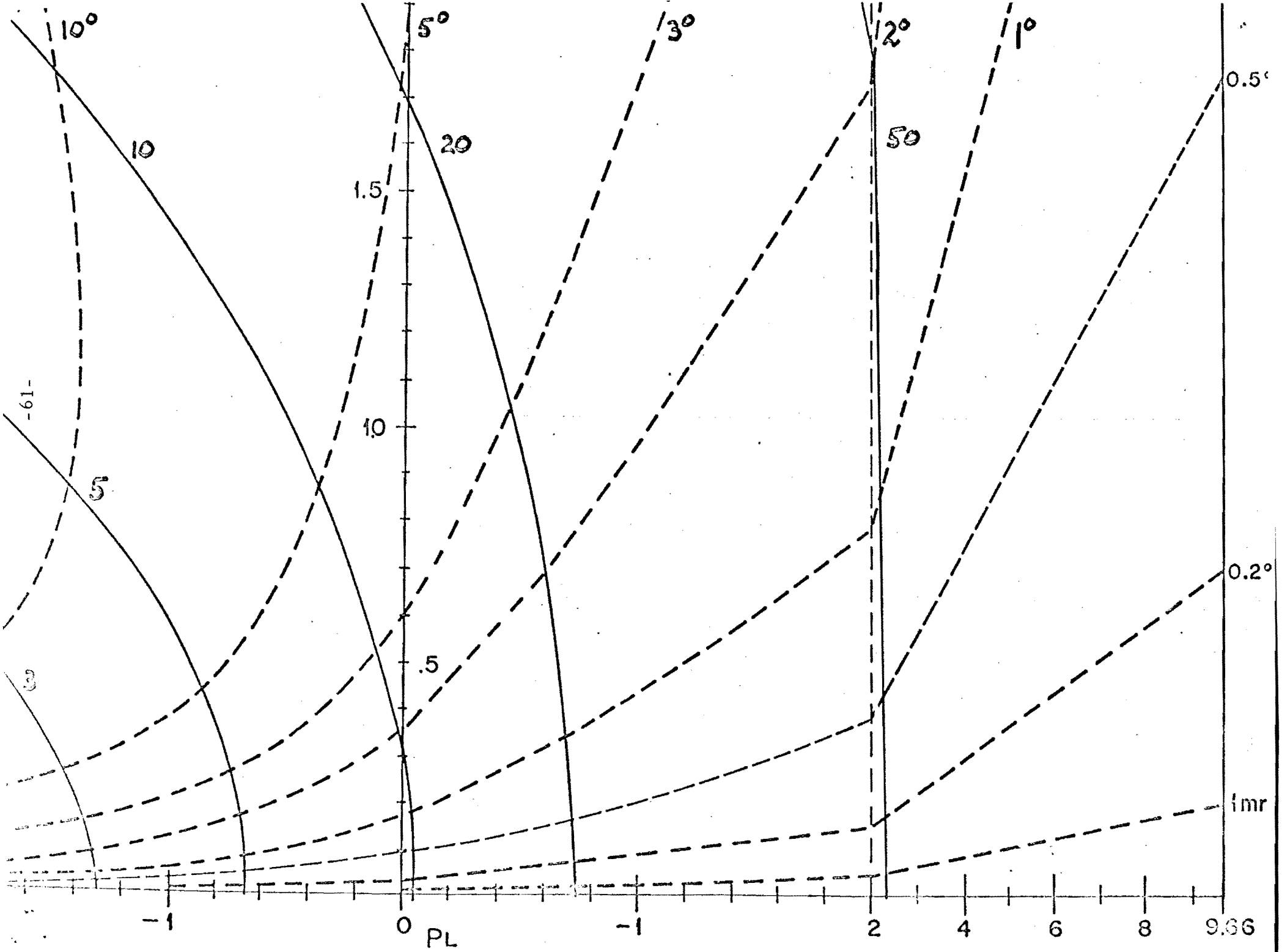




FIG. 4

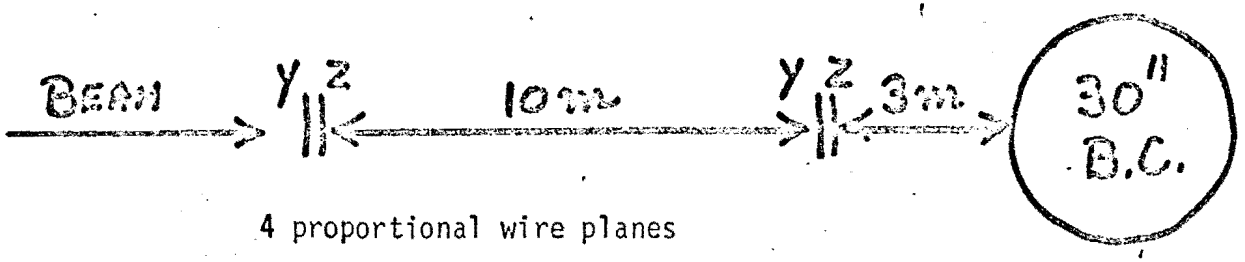


4 proportional wire planes

1 mm wire spacing

2"x2", 50 wires. This can be scaled up by a factor 2 in y if needed.

The momentum defining proportional chamber is not shown, being over 1000' upstream at a focus where the image of the target is ∿2 mm in size. The dispersion is ∿2 "/% at this point.

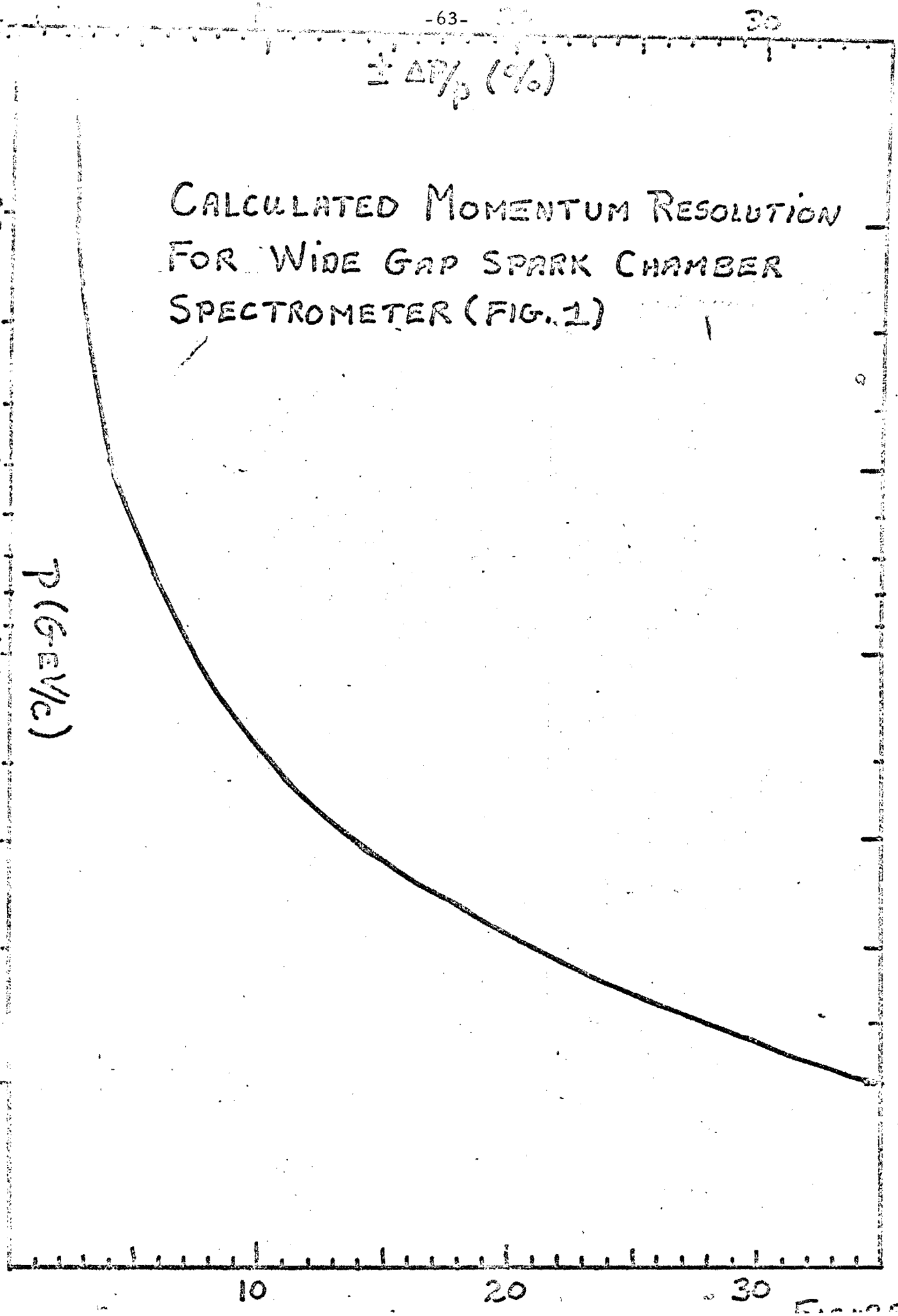


CALCULATED MOMENTUM RESOLUTION FOR WIDE GAP SPARK CHAMBER SPECTROMETER (FIG. 1)

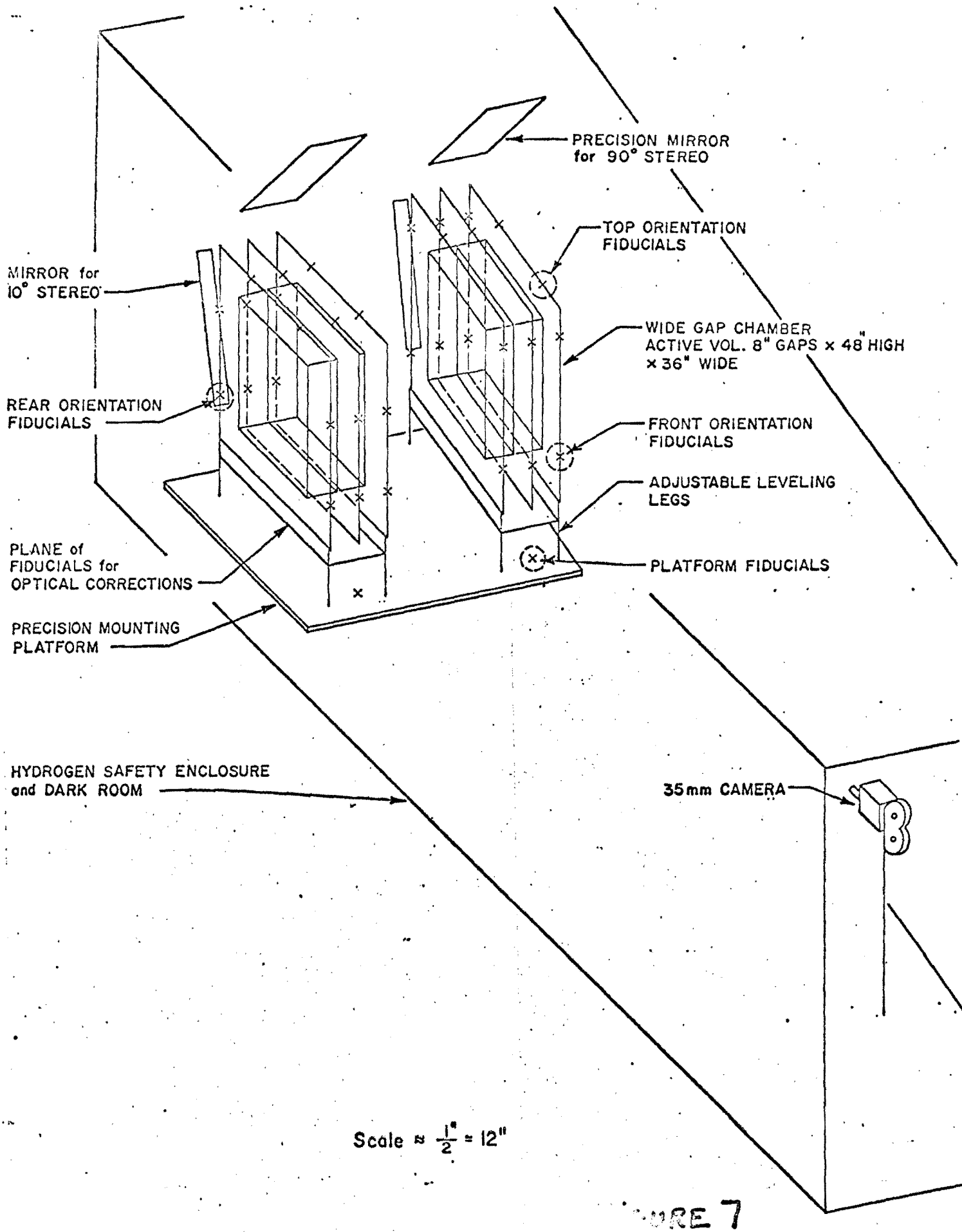


Scale ≈ $\frac{1}{2}$" = 12"

URE 7

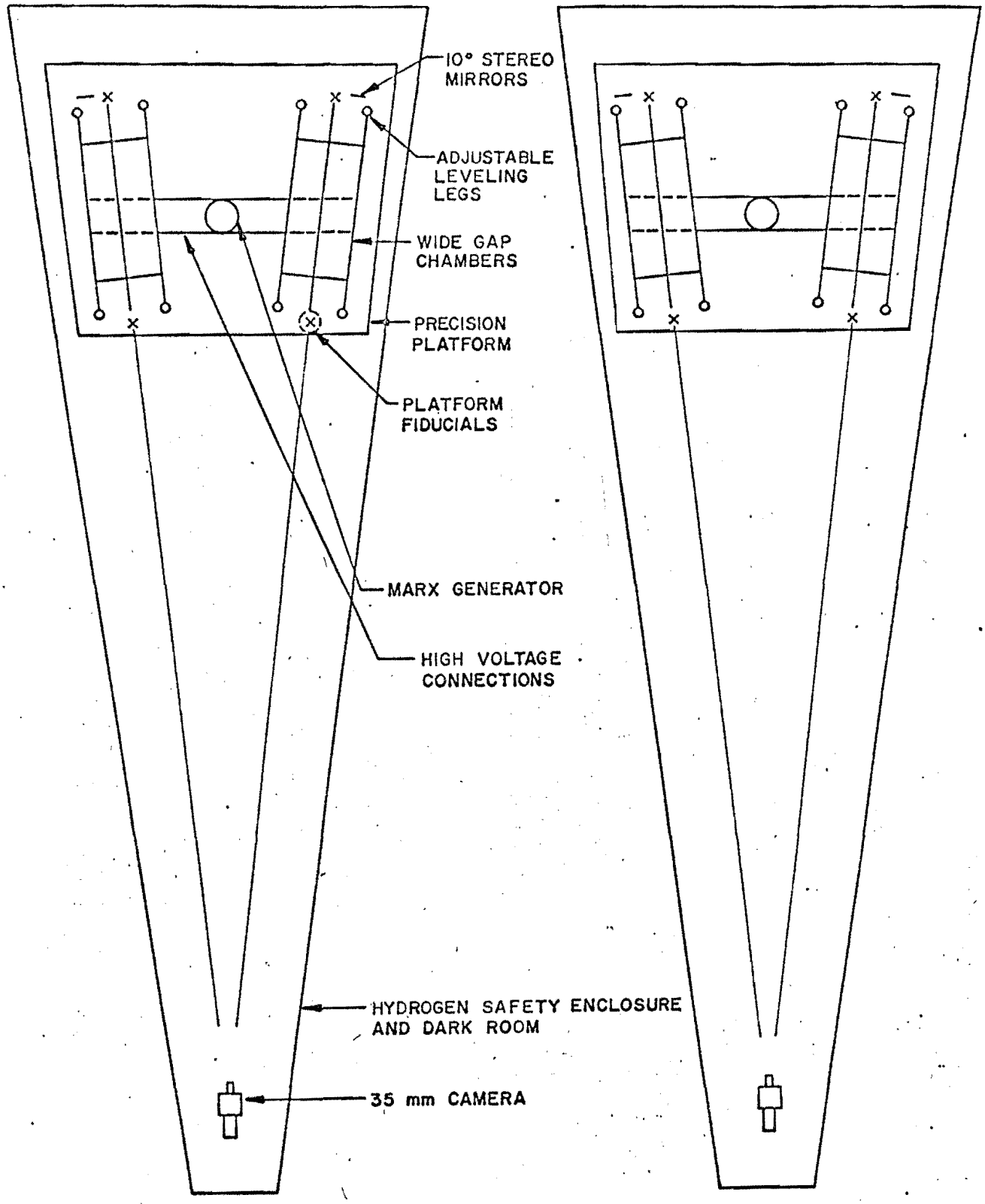


PLAN VIEW
SCALE ≈ $\frac{1}{2}$" = 12"

FIGURE 8

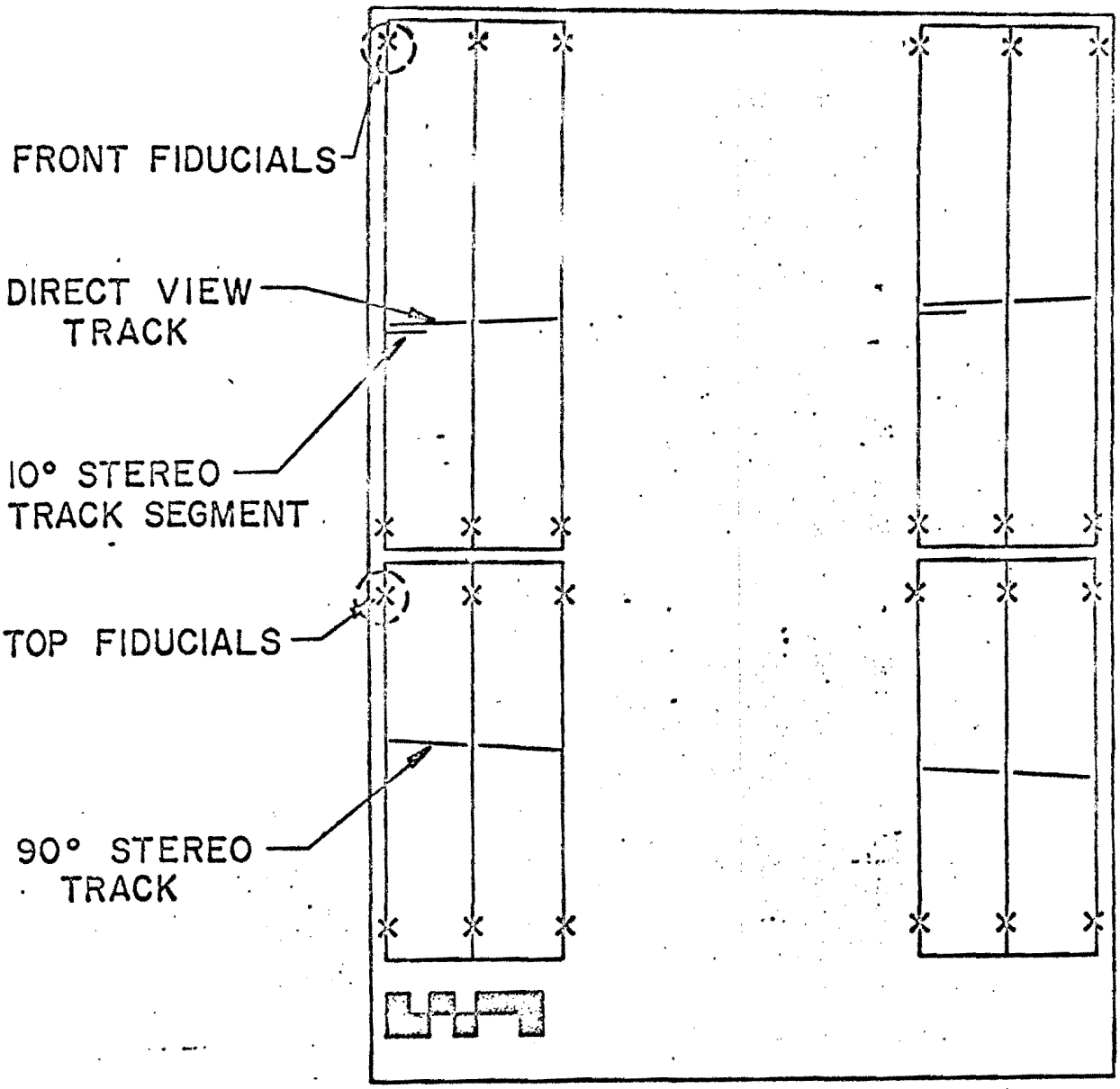


FILM FORMAT 35 mm 1.5" × 1.0"

FIGURE 9

## V. PICTURE REQUIREMENTS

We are requesting an exposure equivalent to 300,000 pictures with an average of 10 tracks per picture in the bubble chamber. In order to determine the number of pictures required, we have assumed an average of 10 tracks per picture, a total cross section of 24 mb, a fiducial length of 15 in. to allow sufficient length for measurement of lower-momentum tracks ($\lesssim$20 GeV/c) in the bubble chamber, and an average charged-track multiplicity which varies as ln s. In order to determine the number of measurable tracks we have extrapolated from our observations at 8 and 18.5 GeV/c. In addition we have assumed reasonable distributions of longitudinal and transverse momentum based on our experience at these lower energies. The requested exposure at 300 GeV/c is expected to yield a total of about 96K events. The average negative-track multiplicity is predicted to be 3.7 and the total average charged-track multiplicity to be 7.4. Thus we expect a total of 355K negative tracks and a total of 710K charged tracks.

Essentially all of the tracks will be measurable with some degree of accuracy. If we limit ourselves to negative tracks for which $\Delta p/p \lesssim 10\%$ ($p_{lab} \lesssim 140$ GeV/c; maximum $x \sim +.47$, and maximum $\Delta x \sim .047$) we will have an estimated 310K measurable negative tracks. This number should be sufficient for a study of the correlations between x, Q, and n at $s = 564$ GeV$^2$. Measurement of the tracks with $x > +.47$ will be possible, but the absolute error on p and on x will be larger, ranging up to $\Delta p/p \sim 21\%$ at 300 GeV/c.

The requested exposure will yield good statistics over a large range

of transverse momentum for the smaller-multiplicity topologies. It will also be sufficient to provide a reasonable estimate of the characteristics of the less-common high-multiplicity events.

# VI. ANALYSIS

## A. Measuring Facility

The Notre Dame measuring facility is capable of fast, efficient data reduction on this experiment. We have measured events in "inclusive" reactions at lower energy and are geared up for doing measurements of this type. We have considerable experience with the 30-in. chamber. (We have published four papers based on 30-in. chamber data.) Thus we will be able to analyze the data without delays for debugging reconstruction programs.

The measuring system used consists of five measuring machines on-line to a DDP-124 operating 16 hurs./day, 5 days/week. We have measured 120,000 tracks in 25 weeks on an "inclusive" experiment at lower energy. (Much of this work was done with only 4 machines, while improved film-transports were being installed.) We are now operating at a rate of 8,000 tracks/week (prescanned film) and quote the previous experiment's rates only as a lower limit to our capability. Four magnetic tape transports can be used for output and for coordination of information from the various portions of the experimental apparatus. The measuring machines have been used efficiently to measure optical-spark-chamber pictures as well as bubble-chamber pictures.

The Notre Dame scanning and measuring staff is familiar with the techniques used in measurement of tracks for an "inclusive" experiment. The combination of conventional measuring machines and trained operators is highly efficient for the proposed experiment, since the operators can be trained to make decisions which are difficult to program.

Trained operators are also very capable of distinguishing among closely-spaced tracks. The real-time interaction between on-line computer and operator is of great value. For example, in cases where the curvature of a track is hard to distinguish, a simple on-line reconstruction can be performed and the results immediately presented to the measurer. For rapid scanning, we are equipped with a system for putting results from scan tables directly on magnetic tape. The information can be immediately supplied to the measurer via the on-line computer. This facility should prove useful for analyzing the wide-gap spark chamber pictures as well as for the bubble chamber pictures. It should be possible to coordinate, via the on-line computer, information about the spark-chamber measurements while measuring the bubble-chamber events, or bubble-chamber information while measuring spark-chamber pictures if this proves necessary. Information on magnetic tape from the upstream proportional chambers and Cerenkov counter can be integrated with other measurements at the same time.

Checks of the data analysis system will be made in advance, so immediate reduction of the data can begin when the experiment is run. We hope that the system will have been previously checked out on measurements of events in the "bare" bubble chamber at several incident energies. We would then have advance knowledge of problems which could arise in handling events in this new energy range and could prepare to handle them. We believe preliminary results on the "inclusive" reactions could be available within 2-3 months after the acquisition of data.

B. Resolution

The resolution of the downstream wide-gap optical spark chamber spectrometer has been discussed in Section IV. It will provide adequate momentum resolution for forward tracks passing through the spectrometer. For example, $\Delta p/p$ will be 10% for tracks with $p_{lab}$ = 140 GeV/c and significantly less for tracks with lower momenta. For tracks with $p_{lab}$ greater than 140 GeV/c the momentum resolution is worse, rising to ~ 21% for $p_{lab}$ = 300 GeV/c. Thus, for a high-precision study of tracks with large positive x and of beam fragmentation, it will be desirable to augment the downstream spectrometer at a later date by adding a magnet and an additional spark-chamber module as suggested in Section IV. C. This would provide improved resolution for very fast forward tracks.

The resolution of the spectrometer in transverse momentum is critically dependent not only on the momentum resolution but on the resolution of the angles for both beam particle and secondary track at the vertex. The angle resolution for the beam particle should be $\approx 10^{-4}$ radian with the proposed beam tagging instrumentation. The angle resolution for the outgoing tracks will depend on the accuracy with which the magnetic field is known. Direct measurements of the angle in the bubble chamber will have a resolution $\approx$ 1mrad. Thus it will be necessary to determine this angle from measurements in the downstream spectrometer plus a measurement of the event vertex if full advantage is to be taken of the system. If an angle resolution of .2 mrad can be achieved, $\Delta Q$ will be less than ~ 100 MeV/c for all

tracks with $Q < 1$ GeV/c and $p_{lab} < 140$ GeV/c.

For most tracks with $p_{lab}$ below about 20 GeV/c it will be necessary to rely on measurements in the bubble chamber alone. We have considered the resolution obtainable in the 30-in. bubble chamber and find it adequate. In Fig. 1 we show the estimated resolution in $p_{lab}$ as a function of $p_{lab}$. These errors are for flat tracks and use the expression for conventional measuring machines with optimized measurements given by Fischer[1]:

$$\frac{\Delta p}{p} = \left[ \frac{3.55\, p^2 \epsilon^2}{H^2 L^2} + \frac{.133a}{H^2 L} \right]^{1/2}$$

where p is the momentum in GeV/c, $\epsilon$ is the point setting error in microns, L is the length of the track in cm., H is the magnetic field in kilogauss, and $a = \ln(4.8\, p) + \ln(145\, p/mc)$. The curve is calculated for relativistic pions ($\beta \approx 1$) with p in GeV/c, $\epsilon = 100\mu$, H = 32 kilogauss, and L = 15". (Since the 30-in. chamber may operate initially at a lower value of H, this figure should be scaled accordingly. However the value $\epsilon = 100\mu$ is conservative and 15" is near the minimum track length for forward tracks, so the results of the figure should be qualitatively correct in any case.) We find $(\Delta p/p) < 8.2\%$ for $p_{lab} < 20$ GeV/c.

The resolution in the transverse momentum Q depends on how well one measures p, the momentum of the secondary track, $\theta$, the laboratory angle of the secondary track, and $\theta_B$, the angle of the beam track. We have estimates the resolution $\Delta Q$ as a function of Q for various laboratory momenta as shown in Fig. 2. In this calculation, an uncertainty in the beam angle of 0.4 mrad is assumed -- comparable to the full spread expected for the beam. In the proposed experiment, proportional chambers should provide a beam uncertainty of about .1 mrad, so this is an

overestimate. Again $\epsilon$ is taken to be 100$\mu$ and the outgoing track is assumed to be flat and 15" in length. These assumptions lead to an uncertainty in secondary track angle of 1.0 mrad for all secondary momenta above about 1 GeV/c. Despite the assumption of flat tracks, the estimates of $\Delta Q$ shown here are conservative since $\epsilon$ may well be less than 100$\mu$ and the average track length greater than 15". Thus the transverse momentum resolution for $p_{lab} \lesssim 20$ GeV/c in the bubble chamber will be comparable to that obtainable in the downstream spectrometer for tracks of higher momentum.

## REFERENCES FOR SECTION VI

[1] C. M. Fisher, "Optimization of Bubble Chamber Design Parameters; Measuring Accuracies for Charged Particles," International Colloquium on Bubble Chambers, April, 1967, CERN 67-26 pp. 25-47.

## FIGURES FOR SECTION VI

Fig. 1. Momentum resolution, ($\Delta p/p$), for relativistic tracks in the 30-in. hydrogen bubble chamber. Calculations are described in the text.

Fig. 2. Resolution in transverse momentum Q as a function of Q for relativistic tracks in the 30-in. hydrogen bubble chamber. Curves are shown for laboratory momenta of 5, 10, 15 and 20 GeV/c. Calculations are described in the text.

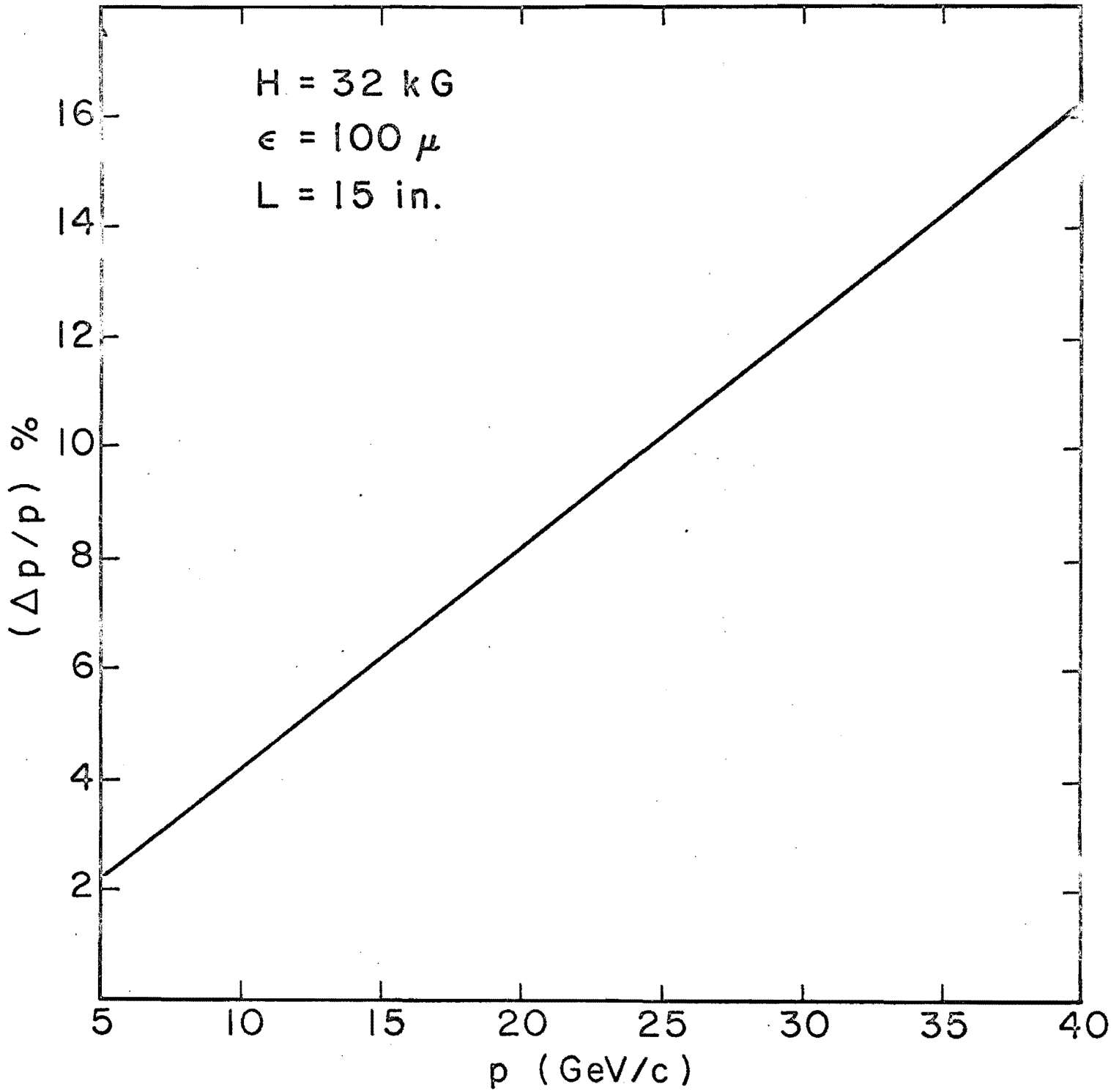
H = 32 kG
ϵ = 100 μ
L = 15 in.
(Δp/p) %
16
14
12
10
8
6
4
2
5
10
15
20
25
30
35
40
p (GeV/c)

Fig. 1

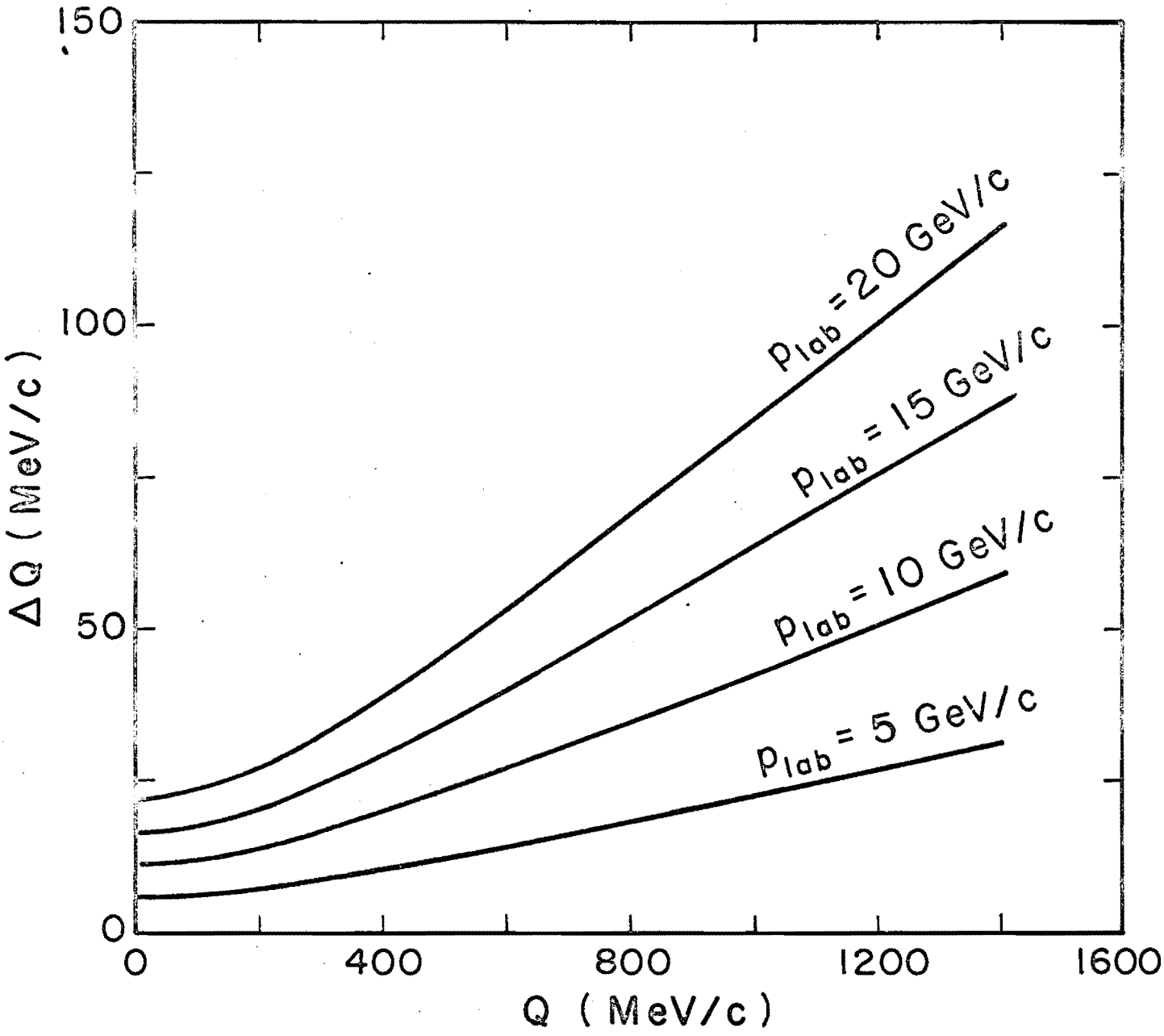
150
100
50
0
ΔQ ( MeV/c )
0
400
800
1200
1600
Q ( MeV/c )
$p_{lab}$ = 20 GeV/c
$p_{lab}$ = 15 GeV/c
$p_{lab}$ = 10 GeV/c
$p_{lab}$ = 5 GeV/c

Fig. 2